A ROBUST VOLTAGE CONTROL METHOD FOR UNIVERSAL EV BATTERY CHARGER LLC RESONANT CONVERTERS

A Thesis

by

Yılmaz Daş

Submitted to the
Graduate School of Sciences and Engineering
In Partial Fulfillment of the Requirements for
the Degree of

Master of Science

in the
Department of Electrical and Electronics Engineering

Özyeğin University
December 2018

A ROBUST VOLTAGE CONTROL METHOD FOR UNIVERSAL EV BATTERY CHARGER LLC RESONANT CONVERTERS

Approved by:

Asst. Prof. Ahmet TEKİN, Advisor,
Department of Electrical and
Electronics Engineering
Özyeğin University

Asst. Prof. Göktürk POYRAZOĞLU,
Department of Electrical and
Electronics Engineering
Özyeğin University

Asst. Prof. Özkan AKIN,
Department of Electrical and
Electronics Engineering
Ege University

Date Approved: 17 December 2018

To my family and memory of my grandmother

ABSTRACT

In this study, a novel control method for LLC resonant converter with wide output voltage range and constant switching frequency is proposed targeting wide range of Electric Vehicle (EV) battery charger standards. In conventional LLC converter control topologies, in order to reach lower output voltage levels, switching frequency happens to move away from the resonance frequency, increasing in most of the cases. However, the switching losses due to switching devices start to become the main bottleneck at high switching frequency operation. In the proposed control method, the switching losses can be reduced by changing duty ratio of PWM driver signals with constant switching frequency operation. High switching frequency operation may cause irreversible inrush current damage at the input terminals during the start-up with corresponding overshoot at the output voltage as well, risking the clients on this particular supply. During soft start, the excessive inrush current can be eliminated by controlling dead time duration of PWM signals in proposed method. The work presented in this thesis proposes a robust and reliable control solution for these particular resonant converter drawbacks. Theoretical analysis for both conventional and proposed control methods are presented in detail. In order to show the effectiveness of the proposed technique, performance metrics of the both are compared experimentally on an LLC resonant converter specification having an output voltage range of 150-500 V with a maximum output power of 7.5 kW.

ÖZET

Bu çalışmada elektrikli araçlar batarya şarj cihazlarının standartları temel alınarak geniş çıkış gerilimi aralığına sahip ve sabit frekans çalışabilen LLC resonant dc/dc çeviriciler için yeni kontrol methodu sunulmuştur. LLC dönüştürücüler için kullanılan mevcut yöntemlerin çoğunda düşük seviyelerde çıkış gerilimi elde edebilmek için anahtarlama frekansı resonans noktasından daha büyük noktalara doğru kaydırılır. Ancak bu bölgelerde anahtarlama kayıpları yüksek frekans çalışmasından dolayı ana problem olmaktadır. Önerilen kontrol yöntemi ile sabit anahtarlama frekasında pwm sürücü sinyallerinin iletim süreleri ayarlanarak anahtarlama kayıpları azaltılabilir. Ek olarak yüksek frekansta anahtarlama yapmak, sistemin yumuşak başlangıç yaptığı zamanlarda kaçınılmaz ani artan akımlara ve buna bağlı çıkış geriliminin hedef seviyeyi aşması gibi kullanıcıya da risk oluşturabilecek problemlere yol açmaktadır. Önerilen yöntem ile yumuşak başlangıç esnasındaki ani yıkıcı akımlar sürücü sinyallerinin sıfır zaman süreleri kontrol edilerek yok edilebilir. Bu tezde sunulan çalışma, resonant çeviricilerin yukarıda bahsedilen problemlerine güçlü ve güvenilir bir kontrol yöntemini çözüm olarak önermektedir. Hem geleneksel hem de önerilen kontrol yöntemi için teorik analizler detaylı olarak sunulmuştur. Önerilen tekniğin avantajını gösterebilmek için her iki yöntemin performans parametreleri 150-500 V çıkış gerilim aralığına ve maksimum 7.5 kW çıkış gücüne sahip bir LLC resonant dönüştürücü üzerinde karşılaştırılmıştır.

ACKNOWLEDGMENTS

Firstly I would like to thank my advisor Asst. Prof. Ahmet Tekin for his suggestions and cooperation during my studies. His knowledge, comments and guidance are most valuable during my studies and will also help me in future.

I am grateful to my second advisor Assoc. Prof. Mutlu Boztepe. His theoretical knowledge always helps me to understand the power electronics in detail. His experience and guidance make me better researcher and designer.

My other colleagues in Vestel Electronics R&D department are helpful to my studies as well. I would like to thank Cengiz Tarhan who is team leader of the power electronics design group for his countless help.

Special thanks to my wife Nezihe Daş and my daughter Meryem Ece Daş for her continuous encouragement and patience. Also I would like to thank my parents for their support.

TABLE OF CONTENTS

ABSTRACT ..... **iv**

ÖZETÇE ..... **v**

ACKNOWLEDGMENTS ..... **vi**

LIST OF TABLES ..... **ix**

LIST OF FIGURES ..... **x**

I INTRODUCTION **1**

1.1 Electric Vehicle Charging Modes 1

1.2 DC-DC Power Conversion 3

1.3 Isolated DC-DC Converter Topologies 7

1.4 Thesis Objectives and Layout 14

II THEORY **16**

2.1 Design Methodology of LLC Resonant Converter 16

2.2 Conventional Constant On Time Control Method for LLC Resonant Converter 36

2.3 Proposed Control Method for LLC Resonant Converter 39

2.4 Loss Analysis of Proposed and Control Method for LLC Resonant Converter 40

2.4.1 Power Losses in Proposed Control Method……42

2.4.2 Power Losses in Conventional Control Method…….44

III DESIGN AND ANALYSIS OF LLC RESONANT CONVERTER……45

3.1 Implementation of the Desing Methodology 45

3.2 Improved Soft Start Characteristics with Proposed Method.....52

3.3 Loss Comparison of a Low Side Mosfet for Both Methods 57

IV CONCLUSION 66

APPENDIX A -SOME ANCILLARY STUFF.....67

BIBLIOGRAPHY 70

VITA 73

LIST OF TABLES

Table 1.1: IEC61851-1 Charging Modes…….3
Table 3.1: System design specification of the LLC resonant converter…….46
Table 3.2: Resonant network parameters of the LLC resonant converter……..49
Table 3.3: The Selected Mosfet Parameters for Loss Comparison……....58
Table 3.4: Test Steps for Loss Comparison…….…..60

,

LIST OF FIGURES

Figure 1.1: Charging Modes in IEC 61851-1 2
Figure 1.2: Applications of DC-DC converters with corresponding output power and voltage levels 4
Figure 1.3: The power-system architecture of an EV/PHEV with charging station....6
Figure 1.4: General schematic of a non-resonant dc-dc converter 7
Figure 1.5: General schematic of a resonant dc-dc converter 8
Figure 1.6: High power dc-dc converters with galvanic isolation 9
Figure 1.7: The series resonant converter (SRC) with its operating waveforms in continuous conduction mode (CCM) 10
Figure 1.8: The parallel resonant converter (PRC) with its operating waveforms in continuous conduction mode (CCM) 12
Figure 1.9: The LLC converter with its operating waveforms in continuous conduction mode (CCM) 13
Figure 2.1: Schematic representation of the full bridge LLC resonant converter 16
Figure 2.2: Switch network output voltage spectrum 18
Figure 2.3: Frequency spectrum of the resonant network current 18
Figure 2.4: Square wave output voltage of the switch network....19
Figure 2.5: Resonant and switch network current....20
Figure 2.6: Equivalent circuit of the switch network....20
Figure 2.7: Input voltage of the rectifier network and rectifier current 21
Figure 2.8: Actual and filtered waveforms of the Vr(t) 22
Figure 2.9: Rectifier network equivalent circuit 23
Figure 2.10: Linear circuit representation of the resonant network....24
Figure 2.11: Linear circuit representation of the overall network 25
Figure 2.12: DC voltage gain curve of the LLC converter for various Q values 27
Figure 2.13: Capacitive and inductive operation waveforms 28
Figure 2.14: Gain margin for defining minimum switching frequency 29
Figure 2.15: Attainable maximum gain with Q for different m values....30
Figure 2.16: Bobbin without primer-seconder section....34
Figure 2.17: Sectional Bobbin 34
Figure 2.18: Flux density waveform in the transformer....35
Figure 2.19: A Square wave 36
Figure 2.20: AC equivalent circuit of the LLC resonant converter 37
Figure 2.21: A modified square wave 39
Figure 2.22: Switching transition of a switch and associated power a) Symmetrical transition b) Worst-case condition for on-off transition....41
Figure 2.23: Typical switching transition of a MOSFET a) turn-on b) turn-off 42
Figure 3.1: Schematic of the proposed system 45
Figure 3.2: Representation of dc gains....48

Figure 3.3: Voltage gain curve vs switching frequency 49
Figure 3.4: Winding construction of the transformer.....50
Figure 3.5: Winding specification of the transformer 50
Figure 3.6: Electrical characteristics of the transformer 51
Figure 3.7: Winding specification of the resonant inductor 52
Figure 3.8: Soft start waveforms with conventional method 54
Figure 3.9: Soft start waveforms with proposed method.....57
Figure 3.10: Experimental prototype 58
Figure 3.11: S2 drain-source voltage, gate input voltage and primer current with conventional method @ $Pout$ =1600 W, $Vout$=160 V, fsw=130 kHz, α=1 μs.....59
Figure 3.12: S2 drain-source voltage, gate input voltage and primer current with proposed method @ $Pout$ =1600 W, $Vout$=160 V, fsw=80 kHz, α=3.2μs.....59
Figure 3.13: Loss comparison of the conventional and proposed method.....63
Figure 3.14: Measured AC waveforms a) Measured Input Voltage and Input Current of classic control b) Measured Input Voltage and Input Current of proposed control.....65

CHAPTER I

INTRODUCTION

1.1 Electric Vehicle Charging Modes

Electric vehicle (EV) market is one of the most growing markets in the world because of increasing of fossil fuel consumption and air pollution [1]-[3]. Therefore, battery charger applications are growing in parallel to EV market. EV battery chargers can be divided into two groups; which are on-board and off -board chargers. There are 4 charging modes as defined in IEC 61851-1 [3], [4], [5]. Power ratings depend on the type of charging mode for Europe as follows [3],[4],[5].

Mode 1 charging means that the connection of an EV to the AC line through single phase not exceeding 250 V AC or a three phase not exceeding the 480 V AC. Based on the country and standardization, it uses the national plug and socket with the maximum current limit of 16 A. This type of charging provide low load for grid and the car is charged economically using a night rate of power. Rated power level is up to 3.7 kW with 1-Phase AC Connection. Due to no additional infrastructure, this mode is mainly used at homes and offices.

Mode 2 charging refers to the connection of an EV to the AC supply with same limits as in Mode 1. It uses conventional plug and socket with maximum current limit of 32 A with protective earth. The difference with the Mode 1 is that the vehicle inlet and connector present a control pin. The AC side of the charging cable doesn't require a

control pin as the control operation is provided by the control box in the cable control device. This recharge mode is generally used in private facilities.

Mode 3 charging means that the connection of an EV to the AC supplies by using electric vehicle supply equipment (EVSE). Maximum limit of the line current doesn't exceed 63 A. There is an extended communication protocol between EVSE and EV to ensure reliable and safety charging operation. This charging mode is typically used in public charging stations and is supplied from the three phase AC line at 50/60 Hz. It is also called "semi-fast" charging since it allows the battery to charge in a few hours once driver is at work or during an activity.

Mode 4 charging has been presented by the use of off-board chargers. There are special communication protocols such as CAN or PLC depend on the charging standard. There is a power conversion inside the EVSE. Moreover, the AC supply is converted to each DC voltage that the EV may request. Plug on the EVSE provide that only matching EV can be connected. Total charging time is in a range from 20 to 30 minutes. By combining charger having high output power with latest battery technologies, it is possible to charge from 0 to 80 % of battery in less than 5 minutes (Ultra-fast charging).

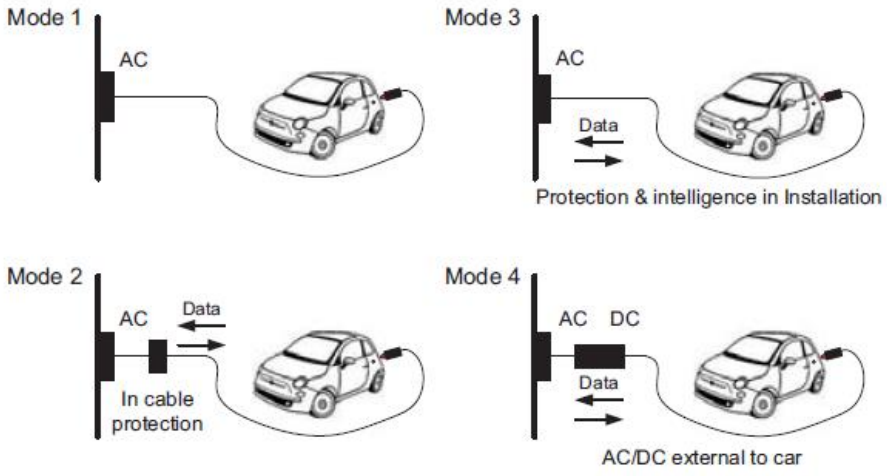

Figure 1.1: Charging Modes in IEC 61851-1

Figure 1.1 shows the representation of the charging modes in IEC 61851-1 standard [4]. Main specifications of the charging modes are provided in Table 1.1 [4].

Table 1.1: IEC61851-1 Charging Modes

Charging Mode	**Maximum Current per Phase**	**Charging Time**	**Vehicle Battery Charger**
Mode 1	16 A	4 ~ 8 h	On Board
Mode 2	32 A	2 ~ 4 h	On Board
Mode 3	63 A	1 ~ 2 h	On Board
Mode 4	400 A DC	5 ~ 30 min	Off Board

1.2 DC-DC Power Conversion

Electrical and electronic products are significant equipment in our life today. All of them involve power conversion to get correct AC or DC form and electrical power level. Electronic circuits which are designed to provide DC voltage required by the electrical and electronic equipment are called as DC-DC converters. Voltage and power levels of the DC-DC converters cover a wide range because of the various applications from low level products such as consumer electronics to high power products such as renewable energy. Figure 1.2 shows the some applications of DC-DC converters [6].

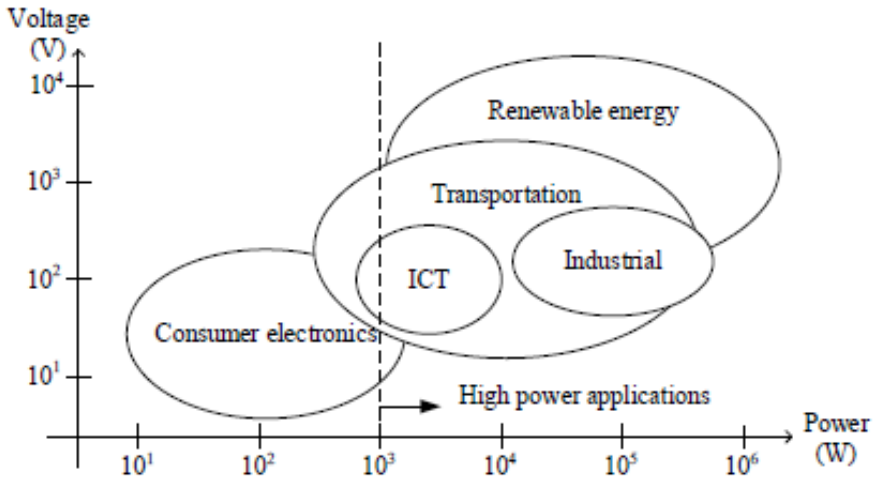

Figure 1.2: Applications of DC-DC converters with corresponding output power and voltage levels

From Figure 1.2, in low power applications, as requiring power level of less than 1 kW, dc-dc converters are utilized generally in consumer electronics such as televisions and IoT (Internet of Things) devices. In high power applications, as requiring power level of more than 1 kW, dc-dc converters are mainly used industrial, transportation, information and communication technologies and renewable energy applications.

Due to adverse effects of increasing fossil fuel consumption, most notably air pollution, great effort has been being made in electrification of transportation system to meet emission standard and to reduce consumption of the fossil fuels. DC-DC converters are mainly used in transportation system such as electric vehicles (EVs), plug-in hybrid electric vehicles (PHEVs), electric trains and electric aircraft. DC-DC converters are in EVs and PHEVs to perform power transfer between electric vehicle supply equipment (EVSE) and batteries and loads. In electric trains, they are utilized as solid state transformer in traction systems [7]. In addition to, they are also used as auxiliary power supply on board for lightning, heating and other loads [8]. In aerospace

field, almost in all system such as mechanical, flying interface, control and hydraulic systems, DC-DC are heavily used to make the systems more compacts, to reduce weight of airplane and to improve fuel consumption. It is possibly in future, airplanes will need more dc-dc converters with higher power ratings since the systems in airplanes are replaced with electric versions [9].

As a result, the dc-dc converters may operate at different conditions. Therefore, in some applications dc-dc converters should accommodate wide load range due to changing loads and voltage variations on the output side. One example of such converters is electric vehicle battery charger applications. There are a lot of electric vehicle charging modes that are mentioned in section 1.1. One of the most important implications of the above regulations is that the charger have to supply wide output voltage range. In order to meet this requirement, the charger should work efficiently at each voltage level which EV battery management system may request. Therefore, the design has to accommodate an appropriate DC to DC converter scheme that operates with high efficiency at each of the power levels providing high power density with overall compact and reliable device size. Therefore highly efficient and high performance dc-dc converter should be used to achieve these targets. The work presented in this thesis proposes a robust and reliable control solution for these particular dc-dc converter drawbacks.

Figure 1.3 represents the power-system architecture of an electric vehicle (EV) and plug-in hybrid vehicle (PHEV) together with charging station [38].

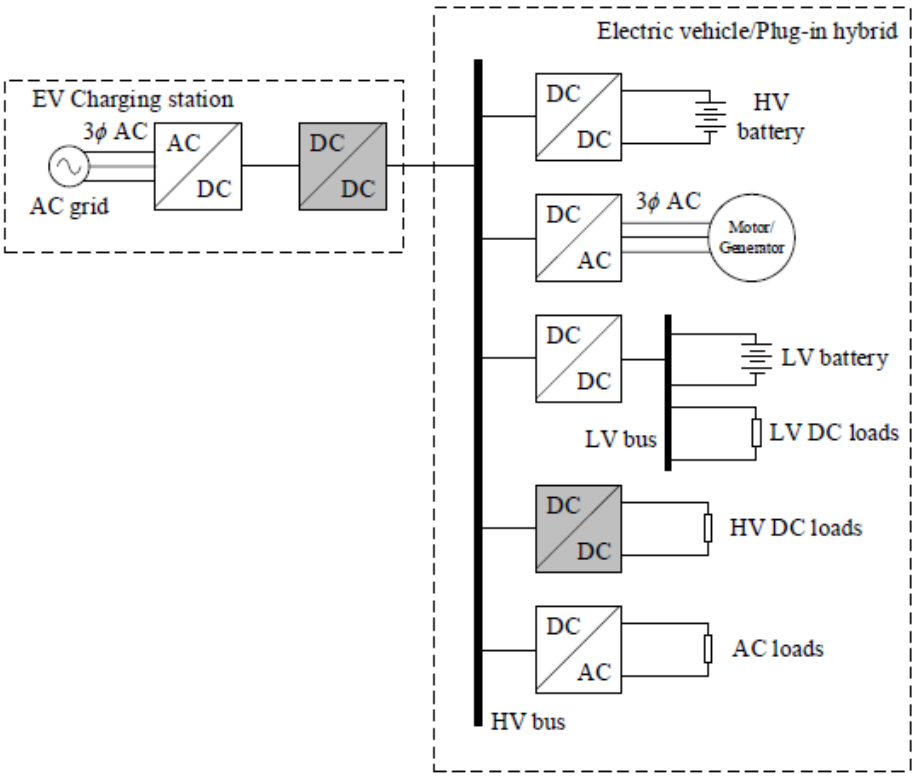

Figure 1.3: The power-system architecture of an EV/PHEV with charging station

The unidirectional converters are highlighted by the grey shading in the figure to show where they are used in the power architecture. In the electric vehicle, high voltage (HV) battery is utilized as power source for motor drive system. As shown in the figure, the system contains high voltage (HV) bus with a voltage up to 800 V [10] and low voltage (LV) bus with a nominal value of 14 V. Bidirectional dc-dc converter is used to charge and discharge the HV battery. The bidirectional converter is also required to get LV bus from the HV bus [11]. The LV battery with a nominal voltage of 12 V supplies power to LV dc loads. The unidirectional dc-dc converter is used as power source to HV dc loads from HV bus. The battery system of the vehicle is charged with dedicated socket and charging station [12] depending on the power capability. A unidirectional dc-dc converter is used in the charging station to charge EV HV batteries. The converter in

charging station and also feeding from DC link obtained by three phase AC utility transfers the power to HV bus in the vehicle. Since the loads and batteries in the vehicle have wide power variations, the dc-dc converters shown in Figure 1.3 accommodate the large load range. In addition to, as the battery need to wide voltage range during charging, the dc-dc converter in the station have to supply wide output voltage range. Providing high power density with overall compact and reliable device size is one of the most important criteria in this operation.

1.3 Isolated DC-DC Converter Topologies

Galvanic isolation in power devices means that the output side of power circuit is electrically and physically isolated from the input side. Electrical isolation is achieved by implementing a transformer to the power circuit. Physical isolation refers to the fact that the secondary wiring doesn't connect to primary wiring. This is a requirement of safety agencies to prevent shock hazard. The transformer can be used to step up or step down voltages depending on its turn ratio between primary and secondary side. Rectifier diodes rectify secondary input voltage and then targeted output voltage is established after filtering with output filter unit. These converters are known as non-resonant converters as depicted in Figure 1.4 [38].

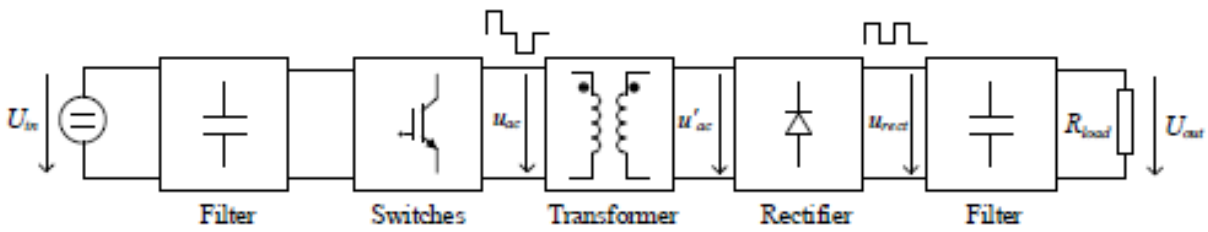

Figure 1.4: General schematic of a non-resonant dc-dc converter

Figure 1.5 shows the schematic resonant dc-dc converter [13]-[15] which reduces the switching losses by allowing soft switching techniques [38]. Since the reduction of switching losses, it enables to operate the dc-dc converter at higher switching frequencies that reduces the size of passive elements and EMI filters. Resonant network consists of resonant capacitance and resonant inductor placed in different combinations before transformer. Here the aim is to filter pulsating input voltage and current of the resonant network generated by switches and to get fundamental harmonics of the waveform so that the switches tur on or turn off at either zero voltage switching (ZVS) and zero current switching (ZCS) respectively. As a result, these are known as soft-switching and used to reduce switching losses and to get better efficiency in the converter. As shown in Figure 1.5, both input voltage of the resonant and secondary rectifier networks have resonant waveform due to filter behavior of the resonant network. Secondary rectifier rectifies the input voltage and after output filter smoothed output voltage is achieved.

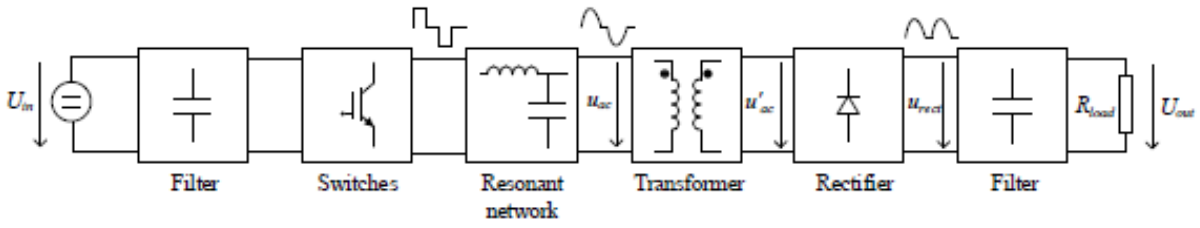

Figure 1.5: General schematic of a resonant dc-dc converter

Resonant topologies are classified as resonant load and resonant switch topologies. Load resonant topologies use combination of resonant network with load [19]-[23]. Resonant load topologies include series resonant converter (SRC) [23], parallel resonant converter (PRC) [23], inductor-inductor-capacitor (LLC) converters [24][25] and inductor-inductor-capacitor (LCC) converters [25][26]. Resonant switch topologies

[27][28] also called as quasi-resonant topologies include quasi-resonant forward and quasi-resonant flyback converters with galvanic isolation. Hybrid topologies use advantages of both resonant and non-resonant converters. Hybrid topologies are classified into two parts that are partial resonant and resonant transitions. Partial resonant topologies operate as both resonant and non-resonant converters during overall switching cycle. In resonant interval, it allows soft switching operation. Partial resonant topologies comprise partial series resonant converter (PSRC) [16], output filter resonant converter (OFRC) [17] and new full bridge hybrid series resonant converter (FB-HSRC). In the resonant transition topologies, resonance only occurs during short commutations between two switches in a phase to turn on at zero voltage. For the rest of time, it operates as non-resonant converters. It can be divided into two sub-parts that are ZVS phase shifted full bridge [16] and auxiliary resonant commutated pole-full bridge [18]. Detailed taxonomy of the converters can be observed in Figure 1.6 [38].

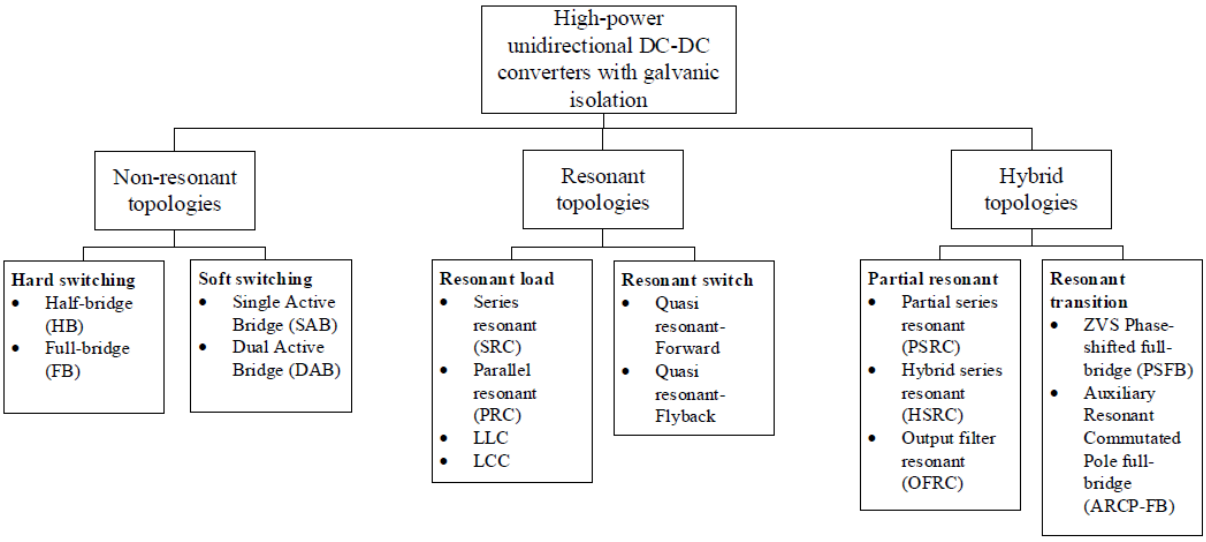

Figure 1.6: High power dc-dc converters with galvanic isolation

The basic form of the load-resonant converters consists of two reactive elements as depicted from Figure 1.5. The series resonant converter (SRC) and parallel resonant converter (PRC) are in this class. In the SRC, L_r and C_r are in series with load at output side. Schematic of SRC and its voltage and current waveform can be shown in Figure 1.7 [38].

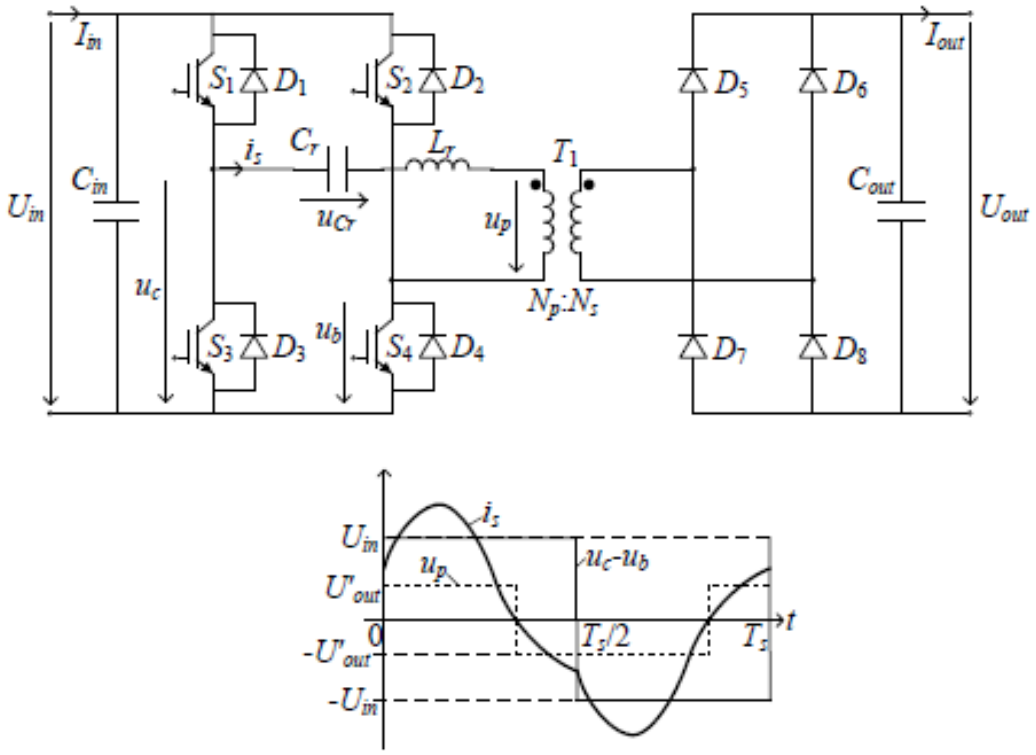

Figure 1.7: The series resonant converter (SRC) with its operating waveforms in continuous conduction mode (CCM)

The resonant frequency of the resonant network is defined as f_{res}

$$f_{res} = \frac{1}{2\pi\sqrt{(C_r L_r)}} \tag{1.1}$$

In the SRC, ZVS or ZCS is achieved during wide load range and wide output voltage operation. Voltage gain can be obtained due to frequency variation with a certain interval. As a result, allowing soft switching operation with various voltage gains provides high efficiency especially at full load points in series-resonant converters. A circulating current flows in SRC and it increases when the load reduces. Therefore the efficiency drops at light loads. As can be observed in Figure 1.7, due to resonance and large swings of the i_s and u_{cr}, peak current stress may occur in C_r and L_r.

In the parallel resonant converter (PRC), resonant capacitor, C_r, is placed as parallel with the load. Its operating waveforms can be depicted in Figure 1.8 [38]. The parallel resonant converter is used as step-up or step-down converter depending on turns ratio of the transformer over a switching frequency range so that this allows to handle wide load range with wide output voltage range. Voltage gain is controlled by changing switching frequency in an interval of a certain range in PRC. Circulating current that doesn't contribute to the power transfer exists even at the no load condition. This is the main reason of the temperature stress in resonant capacitance, resonant inductance and switching devices and so on resulting lower system efficiency. Due to swings at resonant points, highly peak currents occur in resonant network. This is another disadvantage of the PRC similar to SRC. L_o has very large inductance value to smooth load current and provide almost constant current. But it brings extra loss and size to the converter.

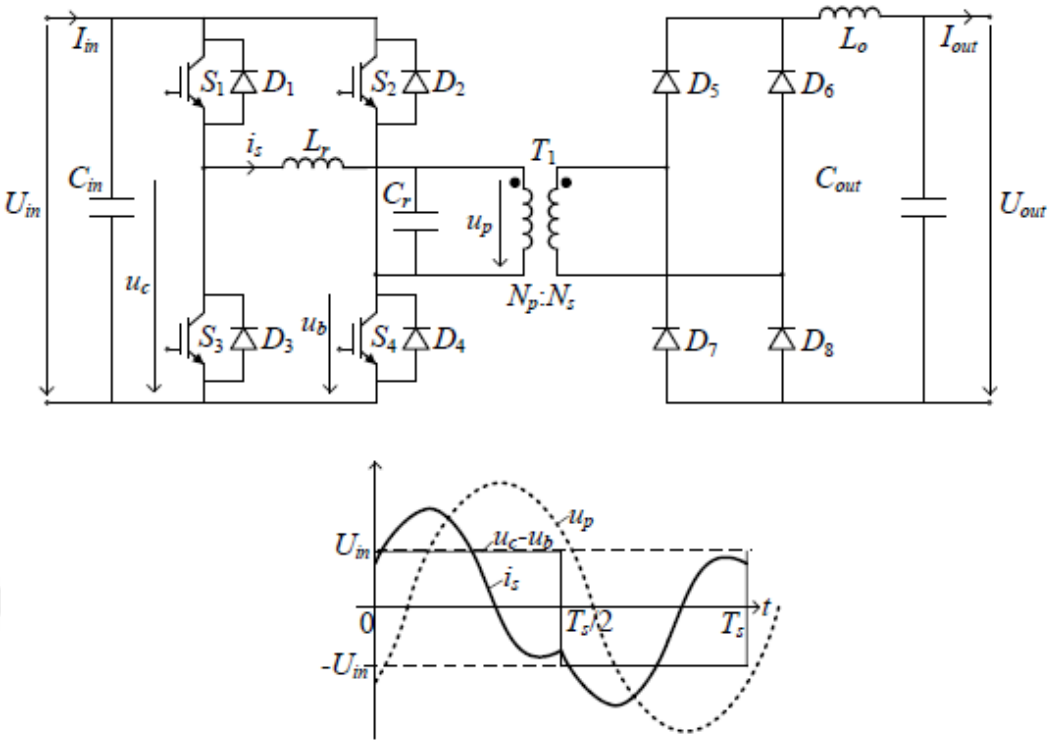

Figure 1.8: The parallel resonant converter (PRC) with its operating waveforms in continuous conduction mode (CCM)

The LCC converter is introduced and presented theoretically in [29]. It has low circulating current and it can operate under no load. Both variable and constant switching frequency control methods can be implemented. Constant switching frequency with phase shifted control is described in [30]. It is generally used for high voltage applications such as high voltage charger [31].

Inductor–inductor–capacitor (LLC) resonant converter is the most popular dc-dc converter for many applications owing to low electromagnetic interference (EMI), ZVS turn on and high efficiency [32]. It is illustrated in Figure 1.9 together with operating waveforms in CCM mode [38].

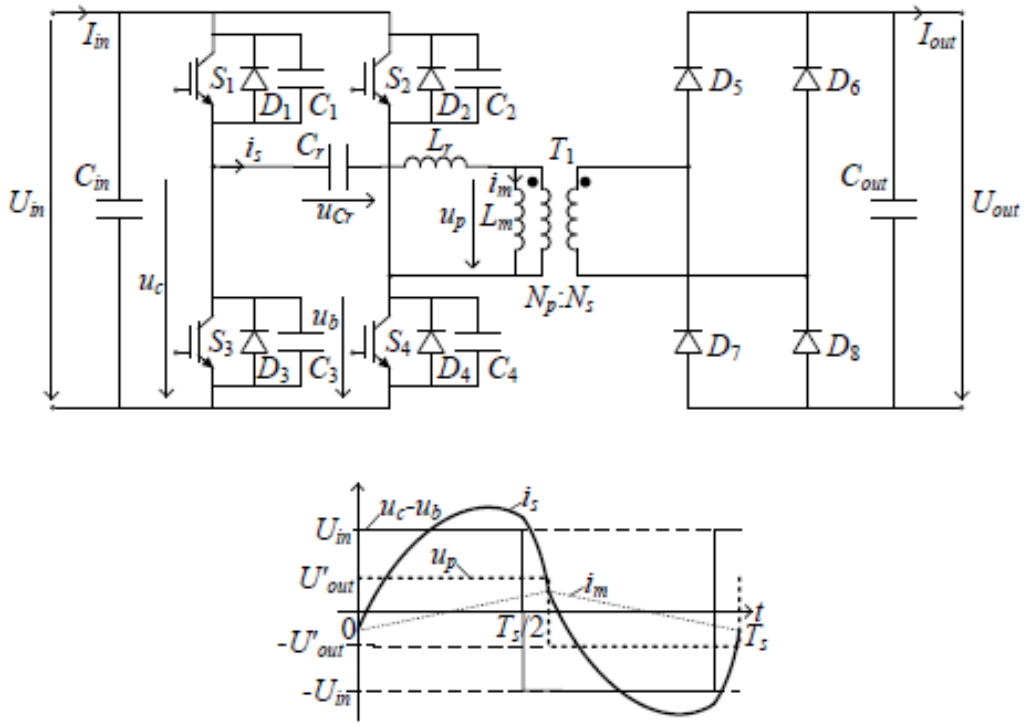

Figure 1.9: The LLC converter with its operating waveforms in continuous conduction mode (CCM)

Outstanding advantages of the LLC converters which allow to operate under ZVS for primary switching devices and allow to operate under ZCS for the secondary rectifier diodes help designer reach high efficiency and power density. The main advantage of the LLC converter is that besides the ZVS turn-on in CCM, ZVS turn-on for primary switching devices is also achieved in discontinuous conduction mode (DCM). Energy storing in the magnetizing inductance, L_m, depicted in Figure 1.9 is provide ZVS turn-on even operating in DCM mode. High efficiency and high power density is obtained with soft switching in DCM and CCM mode over operating wide load and wide output voltage range. Similar to other resonant converters, variable switching frequency or constant switching frequency PWM methods can be used in the LLC control algorithm. For an LLC converter [33] to work as a wide output voltage

source, the voltage gain is set according to required output voltage level. Voltage gain is inversely proportional to switching frequency, hence low output voltage levels becomes problematic due to high switching frequency. High switching frequency operation means higher switching losses on switching components which are most commonly MOSFETs and IGBTs. Another point is that the system should start with low voltage gain in order to eliminate excessive inrush current and high voltage spikes at start up [34][35]. In order to avoid such unexpected dangerous conditions due to parasitic capacitance and stray inductance of the system, initial switching frequency starts from high value and then decreases progressively until the final desired output voltage level is established. During start up, because of inrush current and high switching frequency with the stray inductances on the physical layout of circuit and self-inductance of the MOSFET itself, high voltage spikes can occur at the drain-source junction [36]. Once this voltage spike is higher than breakdown voltage of the MOSFET, the device enters avalanche mode [36][37]. In this mode, the device experiences large avalanche current that may result in permanent damage [36].

1.4 Thesis Objectives and Layout

In this thesis, a new control method for the LLC resonant converter is proposed which allows low output voltage levels without going up high in switching frequency. Switching losses are reduced by operating at relatively low switching frequency. Moreover, the circuit is protected from excessive inrush current and high voltage spikes at start up by implementing a soft start procedure in which the MOSFET conduction time is gradually increased from zero to the final value. Since on time of the MOSFET is minimum at start up, high voltage spikes and current peaks are naturally eliminated. Thesis is organized as follows;

Chapter I introduces electric vehicle charging modes in standards. DC-DC power conversion, its applications and usage of it in EV/PHEV are presented. Taxonomy of the isolated dc-dc converter topologies is provided and resonant topologies are classified in detail.

Chapter II gives theoretical analysis for the design steps of the resonant network, conventional control and proposed control method for the LLC converter respectively. In addition to, loss analysis of the both methods for the LLC converter is presented theoretically in detail.

In Chapter III, in order to show the effectiveness of the proposed technique, performance metrics of the both are compared experimentally on an LLC resonant converter specification having an output voltage range of 150-500 V with a maximum output power of 7.5 kW.

Chapter IV concludes the thesis.

CHAPTER II

THEORY

2.1 Design Methodology of LLC Resonant Converter

LLC resonant converter mainly consists of the three stages that are switch network, resonant network and rectifier network respectively. A simplified schematic of the full bridge LLC resonant converter is shown in Figure 2.1. Here, $V_s(t)$ is input voltage at resonant network terminal or output voltage at switch network terminal. $i_s(t)$ the resonant network current in primer side. $V_r(t)$ is input voltage of the rectifier network and $i_r(t)$ is rectifier current in seconder side.

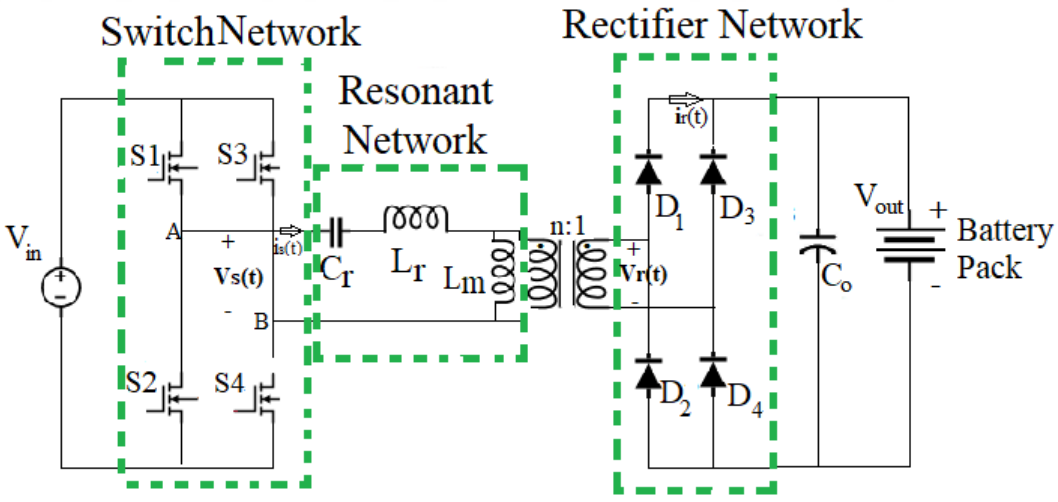

Figure 2.1: Schematic representation of the full bridge LLC resonant converter

Switch network can be full bridge type or half bridge type in LLC topology and full bridge type is commonly implemented in most of high power applications especially in dc fast EV chargers due to provide high power rating. Switching devices

are grouped as S1-S4 and S2-S3 respectively as shown in Figure 2.1. Switch network generates symmetrical square wave having amplitude V_{in} by driving grouped switches alternately with 50 % duty cycle. A dead time is implemented to prevent cross-conduction.

L_m is magnetizing inductance which acts as a shunt inductor, L_r is leakage inductance referred to primary side and C_r is resonant capacitance. Resonant network includes these reactive components. There is an important amount of the magnetizing current in primary side and it doesn't contribute to power transfer. Since the magnetizing current freewheels in primary side of the transformer even at no-load condition, it is disadvantage of the LLC converter. Amount of this current depends on value of L_m. Since L_m is relatively small, it causes that considerable amount of the circulating current flows into primary side.

Secondary stage is designed as full wave rectifier that rectifies secondary input voltage in both positive and negative half periods.

The filtering behavior of the resonant network allows usage of only fundamental harmonic of the square wave resonant network input voltage ($V_s(t)$ as shown in Figure 2.1) that contributes to the power transfer. This approximation is known as fundamental harmonic approximation (FHA) and it ensures simplified sinusoidal AC analysis of the resonant converter to developer.

Frequency spectrum for the output voltage of the switch network, $V_s(t)$, is shown in Figure 2.2 [22].

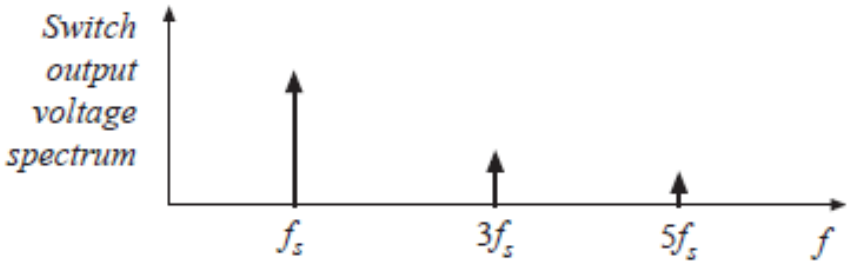

Figure 2.2: Switch network output voltage spectrum

f_s is switching frequency of the switch network. Side harmonics in addition to fundamental harmonic f_s can be shown in spectrum of the output voltage of the switch network.

Since the filtering behavior of the system, only fundamental harmonics of the resonant network current ($i_s(t)$) is observed in Figure 2.3 [22].

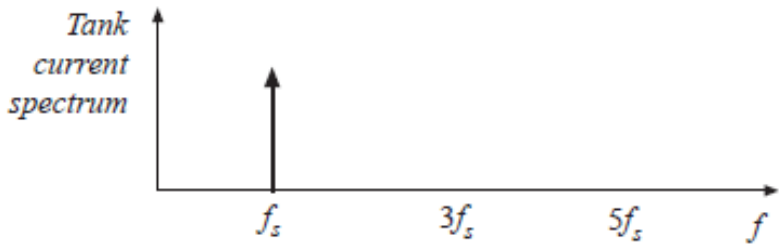

Figure 2.3: Frequency spectrum of the resonant network current.

Output voltage of the switch network, $V_s(t)$, is shown in Figure 2.4 [22]. $V_{s,F}$ is fundamental harmonic of the square wave voltage.

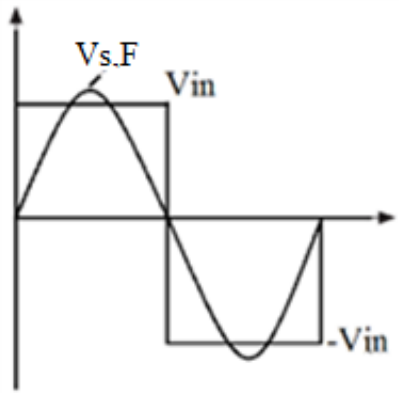

Figure 2.4: Square wave output voltage of the switch network

Fourier series for the output voltage of the switch network can be defined as [39]

$$V_s(t) = \sum_{n\ odd}\left(\frac{4V_{in}}{n\pi}\right)sin(n\omega_0 t) \tag{2.1}$$

The fundamental component is

$$V_{s,F}(t) = \frac{4V_{in}}{\pi} sin(n\omega_s t) = V_{s,F}\ sin(n\omega_s t) \tag{2.2}$$

To obtain average value of the switch network current $i_g(t)$, it is assumed that the resonant network current can be defined as:

$$i_s(t) = I_{s1} sin(\omega_s t - \varphi_s) \tag{2.3}$$

Figure 2.5 shows both resonant current and switch network current in integrated form [22].

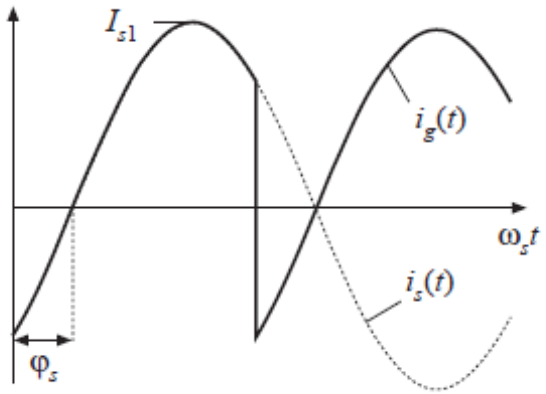

Figure 2.5: Resonant and switch network current

$i_g(t)$ expresses the current for each leg in switch network. Its mean value can be defined as:

$$< i_g(t) >_{Ts} = \frac{2}{T_s}\int_0^{\frac{T_s}{2}} i_g(t)dt$$

$$< i_g(t) >_{Ts} = \frac{2}{T_s}\int_0^{\frac{T_s}{2}} I_{s1} sin(\omega_s t - \varphi_s)\, dt$$

$$< i_g(t) >_{Ts} = \frac{2}{\pi} I_{s1} cos(\varphi_s) \qquad (2.4)$$

Figure 2.6 shows the equivalent circuit of the switch network [22].

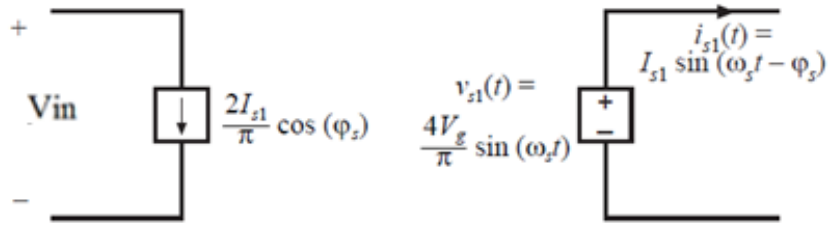

Figure 2.6: Equivalent circuit of the switch network

In order to model rectifier network, it is assumed that there is large output filter having small voltage ripple at the output. $V_r(t)$, input voltage of the rectifier network and $i_r(t)$, rectifier current are shown in Figure 2.7 [22].

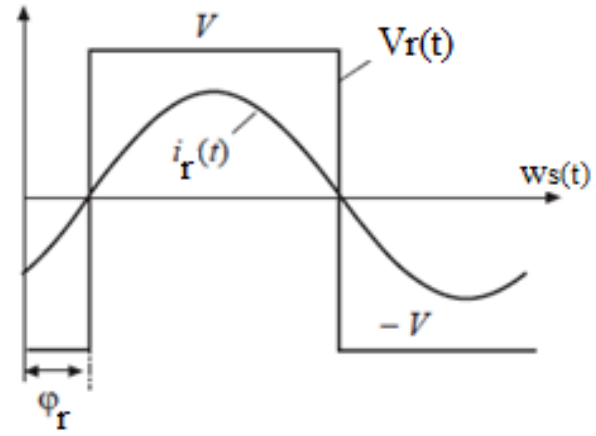

Figure 2.7: Input voltage of the rectifier network and rectifier current

Fourier series for $V_r(t)$, can be defines as:

$$V_r(t) = \sum_{n\ odd}(\frac{4V}{n\pi})sin(n\omega_s t - \varphi_r) \tag{2.5}$$

$i_r(t)$ is in phase with $V_r(t)$ as can be shown in Figure 2.7 and it is expressed as:

$$i_r(t) = I_{r1} si\, n(\omega_s t - \varphi_r) \tag{2.6}$$

Since the resonant network filters the other harmonics except fundamental component of the applied voltage, other harmonics in $V_r(t)$ can be ignored and it is simplified as:

$$V_{r1}(t) = \frac{4V}{\pi} sin(\omega_s t - \varphi_r) = V_{r1} sin(\omega_s t - \varphi_r) \tag{2.7}$$

Actual waveforms and filtered waveforms can be observed in Figure 2.8 [22].

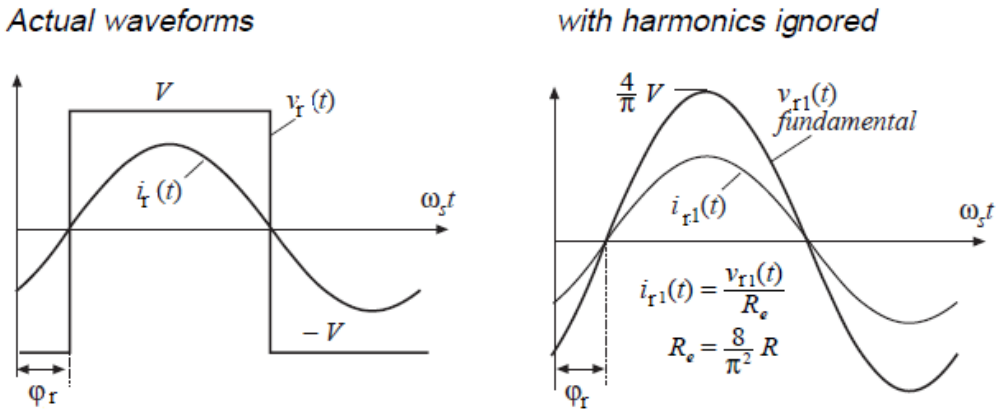

Figure 2.8: Actual and filtered waveforms of the $V_r(t)$

DC output current is equal to mean value of $i_r(t)$ and it is denoted by "I" as follows:

$$< i_r(t) >_{T_s} = I \tag{2.8}$$

Hence

$$< i_g(t) >_{Ts} = \frac{2}{T_s} \int_0^{\frac{T_s}{2}} I_{r1} |sin(\omega_s t - \varphi_r)| \, dt$$

$$< i_g(t) >_{Ts} = \frac{2}{\pi} I_{r1} \tag{2.9}$$

Fundamental harmonics of the rectifier current and voltage are in phase and therefore rectifier network introduces resistive load to resonant network. Equivalent circuit is shown in Figure 2.9 [22].

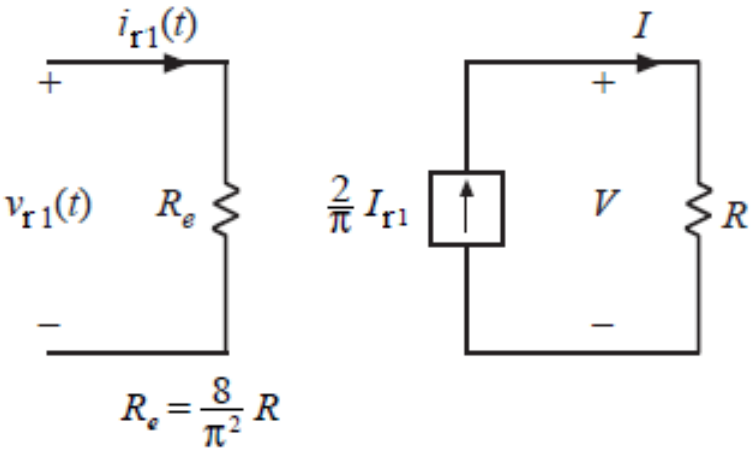

Figure 2.9: Rectifier network equivalent circuit

Since the harmonics in $V_{r1}(t)$ doesn't contribute to power transfer, effective resistance or AC equivalent load resistance can be calculated as

$$R_e = \frac{V_{r1}(t)}{I_{r1}(t)} = \frac{8}{\pi^2}\frac{V}{I}$$

$$R_e = \frac{8}{\pi^2} R = 0.8106R \tag{2.10}$$

Considering the transformer turns ratio ($Np/Ns=n$), effective resistance referred to primer side can be defined as

$$R_e = \frac{8n^2}{\pi^2} R \tag{2.11}$$

Figure 2.10 shows the replaced linear circuit with ac circuit. Resonant network is induced by sinusoidal $V_{s,F}(t)$ and loaded by the equivalent load resistance R_e [22].

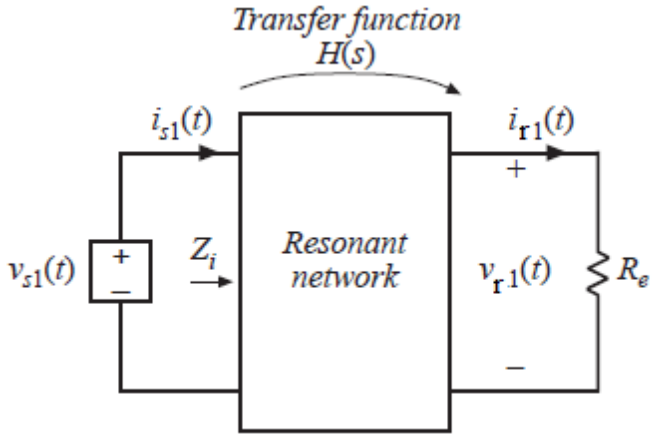

Figure 2.10: Linear circuit representation of the resonant network

To obtain transfer function *H(s)*, conventional linear circuit analysis is made.

$$H(s) = \frac{V_{r1}(s)}{V_{s1}(s)} \tag{2.12}$$

Magnitude of *H(s)* is the ratio of peak values of input and output voltages.

$$|H(s)|_{s=j\omega_s} = \frac{V_{r1}}{V_{s1}} \tag{2.13}$$

Resonant network output current is expressed as

$$i_{r1}(s) = \frac{V_{r1}(s)}{R_e} = \frac{H(s)}{R_e} V_{s1}(s) \tag{2.14}$$

Magnitude of the $i_{r1}(s)$

$$i_{r1} = \frac{|H(s)|_{s=j\omega_s}}{R_e} V_{s1} \tag{2.15}$$

Now, model of the ac circuit is reduced to linear circuit. Figure 2.11 shows this circuit and it is used in calculating voltage gain which is denoted by *M* [22].

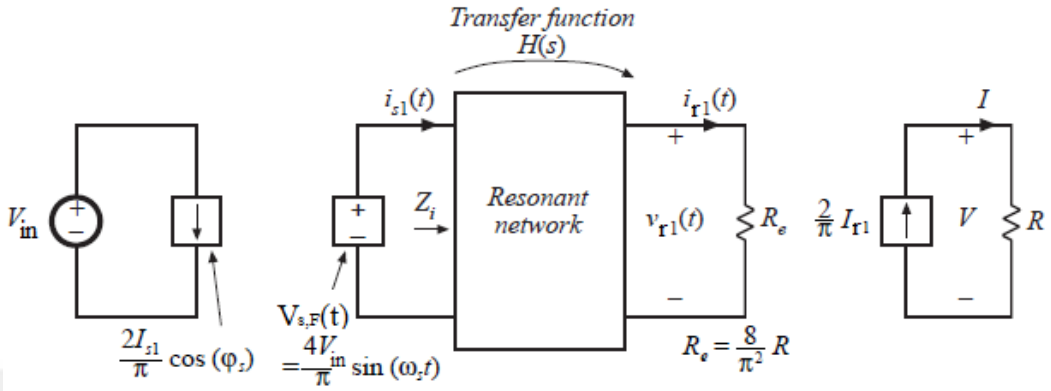

Figure 2.11: Linear circuit representation of the overall network

Voltage gain of the system is defined as follows based on Figure 2.11.

$$M = \frac{V}{V_{in}} = \left(\frac{V}{I}\right)\left(\frac{I}{I_{r1}}\right)\left(\frac{I_{r1}}{V_{r1}}\right)\left(\frac{V_{r1}}{V_{s1}}\right)\left(\frac{V_{s1}}{V_{in}}\right) \tag{2.16}$$

From Figure 2.11, each value is implemented as follows

$$M = \frac{V}{V_{in}} = (R)\left(\frac{2}{\pi}\right)\left(\frac{1}{R_e}\right)\left(|H(s)|_{s=j\omega_s}\right)\left(\frac{4}{\pi}\right) \tag{2.17}$$

Since R_e eliminates $(1/R_e)$ in above formula, consequently *M* is defined as

$$M = \frac{V}{V_{in}} = |H(s)|_{s=j\omega_s} \tag{2.18}$$

So, voltage gain of the system is equal to magnitude of the resonant transfer function that is loaded by the effective resistance R_e. Considering the transformer turns ratio (Np/Ns=n), output voltage shown in primer side is n times V. Therefore M is obtained as

$$M = n\frac{V}{V_{in}} \tag{2.19}$$

The voltage gain is provided based on the FHA technique [40],

$$M(f_n, l, Q) = \frac{1}{\sqrt{\left(1+l-\frac{l}{f_n^2}\right)^2 + Q^2\left(f_n-\frac{1}{f_n}\right)^2}} \tag{2.20}$$

with the following definitions :

DC voltage gain: $M = n\frac{V}{V_{in}}$ (2.21)

Resonant frequency: $f_{res} = \frac{1}{2\pi\sqrt{L_r C_r}}$ (2.22)

Characteristic impedance: $Z_0 = \sqrt{\frac{L_r}{C_r}} = 2\pi f_{res} L_r = \frac{1}{2\pi f_{res} C_r}$ (2.23)

Quality factor: $Q = \frac{Z_0}{R_e} = \frac{\pi^2 I_{out}}{8 V_{out} n^2} Z_0$ (2.24)

Inductance ratio: $l = \frac{L_r}{L_m}$ (2.25)

Normalized frequency: $f_n = \frac{f_s}{f_{res}}$ where f_s denotes the switching frequency (2.26)

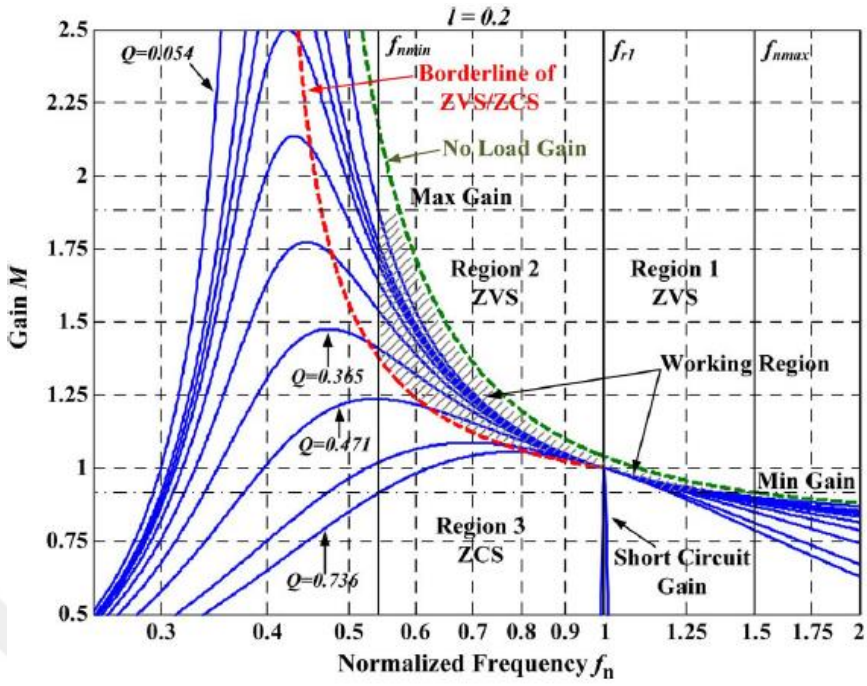

Figure 2.12: DC voltage gain curve of the LLC converter for various Q values

From Figure 2.12 [34], Voltage gain characteristic of the LLC resonant converter is only related to f_s if the load situation and inductance ratio isn't changed. Figure 2.12 shows the dc voltage gain characteristic versus normalized switching frequency for various Q with constant l value of 0.2. It can be clearly seen in Figure 2.12 that voltage gain of the LLC resonant converter is almost independent of the load if the switching frequency is around resonant frequency. At this point the gain is unity regardless of the load variation. This is key advantage of the LLC resonant converter over classic series resonant converters. Therefore if the system has unique output voltage, operating frequency of the converter is set to resonant point that is natural behavior of the developer.

Above the peak gain frequency, impedance of the resonant network becomes inductive and primer current lags the applied voltage as shown in Figure 2.13 [34]. This allows the switching devices to turn on under ZVS operation. However, below the peak gain frequency, impedance of the resonant network becomes capacitive and primer current leads the applied voltage as illustrated in Figure 2.13. This causes noise problems due to reverse recovery of the MOSFET body diode in switching transition. In addition, control algorithm of the output voltage developed for inductive region isn't valid during capacitive operation.

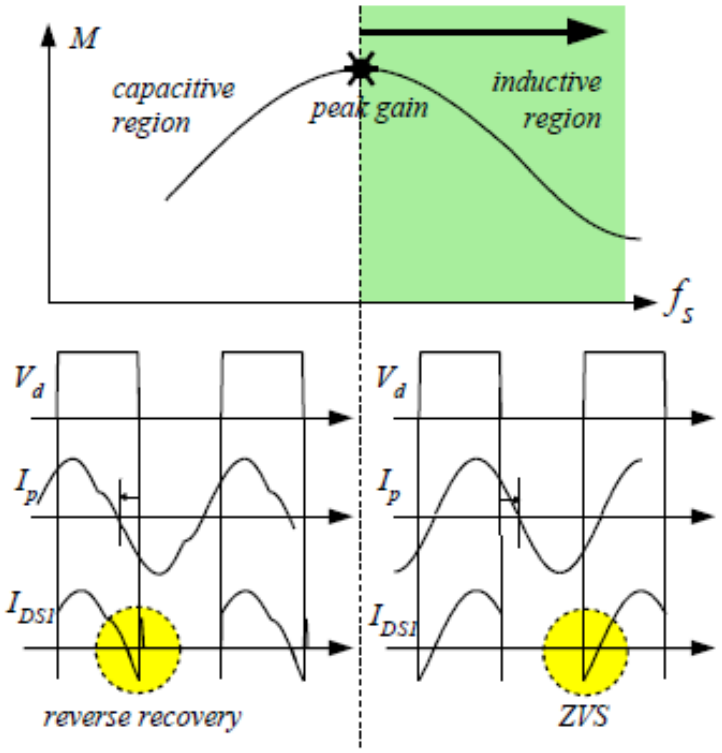

Figure 2.13: Capacitive and inductive operation waveforms

Therefore, inductive region should be selected for overall operation and minimum switching frequency have to be limited to be above the peak gain frequency that guarantees ZVS operation at entire load and output voltage conditions. 10-20% of the maximum peak gain is commonly implemented as a margin during design as depicted in Figure 2.14 [34].

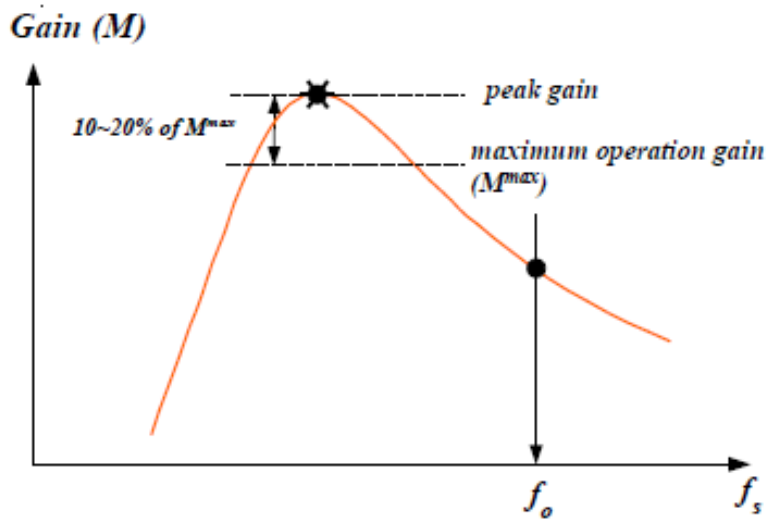

Figure 2.14: Gain margin for defining minimum switching frequency

Figure 2.15 shows variation of attainable maximum gain with Q for different $m = (L_r + L_m)/\ L_r$ values [34].

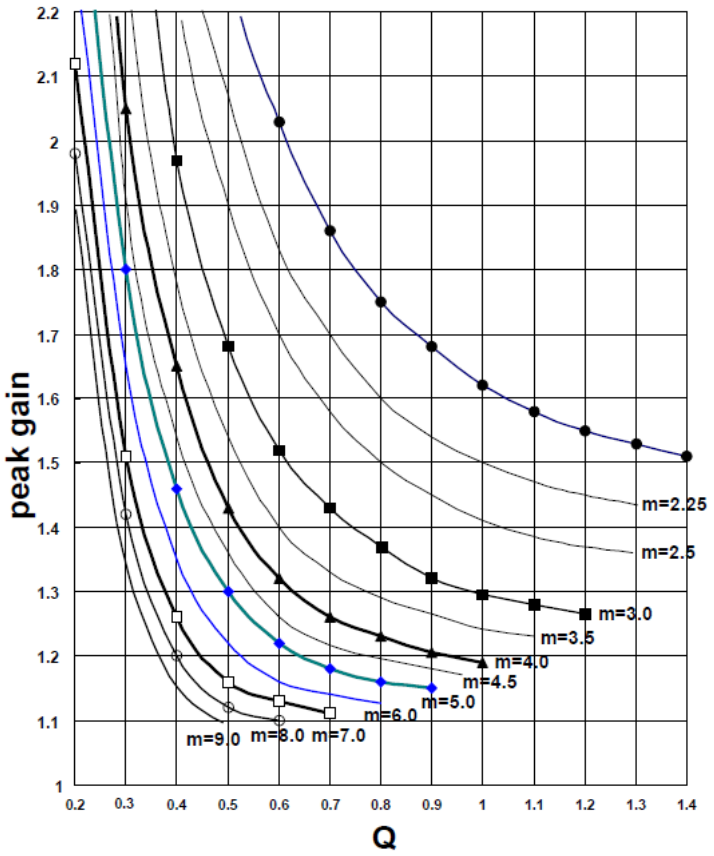

Figure 2.15: Attainable maximum gain with *Q* for different m values

Design steps are presented in below by using Figure 2.1 as a reference [34],[40].

1) Determine system specifications

The efficiency (E_{eff}) of the converter should be estimated to specify maximum input power with a given maximum output power. With a given output power, efficiency of the power converter is defined as:

$$P_{in,max} = \frac{P_{out,max}}{E_{eff}} \tag{2.27}$$

where $P_{in,max}$ is maximum input voltage and $P_{out,max}$ is maximum output voltage.

Secondly, define $V_{in,min}$, $V_{in,max}$, $V_{out,min}$, $V_{out,max}$, $V_{in,nom}$, $V_{out,nom}$ that are minimum input voltage, maximum input voltage, minimum output voltage, maximum output voltage, nominal input voltage and nominal output voltage respectively.

2) Obtain a transformer turns ratio

The minimal transformer turns ratio in Figure 2.1 should be selected at unity gain once input and output voltages are at nominal value and turns ratio is given by:

$$n = \frac{V_{in,nom}}{V_{out,nom}} \tag{2.28}$$

3) Define the minimum, maximum and nominal dc voltage gain of the resonant converter

In order to limit variation of the switching frequency, switching frequency is set to near points of the resonant frequency. Since the maximum output power is given at nominal output voltage, the converter is designed to operate at resonant frequency for maximum output power at nominal output voltage condition. Maximum and minimum voltage gains are defined as follows:

$$M_{max} = \left(\frac{V_{out,max}}{V_{in,min}}\right) n \tag{2.29}$$

$$M_{min} = \left(\frac{V_{out,min}}{V_{in,max}}\right) n \tag{2.30}$$

$$M_{nom} = \frac{V_{in,nom}}{V_{out,nom}} \tag{2.31}$$

M_{nom} is almost unity once the resonant converter operates at resonant frequency.

4) Calculate the effective load resistance

The effective load resistance (R_e) is defined as follows by getting transformer turns ratio in above equation.

$$R_e = \left(\frac{8n^2}{\pi^2}\right)\left(\frac{V_{out}^2}{P_o}\right) \tag{2.32}$$

5) Define resonant network components

In order to design resonant network, right quality factor (Q) should be chosen from peak gain curves illustrated in Figure 2.15 for various m values. m value is chosen in step 2 to provide unity voltage gain at resonant frequency with nominal output voltage condition. Before selecting Q, 10-20% gain margin have to be implemented on maximum voltage gain to maintain ZVS operation at load transients and unexpected conditions. After Q is selected, resonant network parameters are given as:

$$C_r = \frac{1}{2\pi Q f_{res} R_e} \tag{2.33}$$

$$L_r = \frac{1}{(2\pi f_{res})^2 C_r} \tag{2.34}$$

$$L_p = m * L_r \tag{2.35}$$

6) Design the transformer of the resonant converter

After determining the L_p and L_r , these values can be measured in a transformer as well. While L_p is measured in primary-side by making secondary windings open circuit, L_r can be measured in primary terminals together with making primary windings short-circuit. L_r can also be given with discrete core for high power converters, although it is provided with integrated power transformer for low power applications. Thermal limitation on winding elements doesn't allow to get L_r from an integrated transformer in high power applications. Therefore, for the resonant inductor, discrete core should be used in high power converters. So, bobbin without section can be used and one schematic for this type of bobbin can be shown in Figure 2.16. In low power converters, in order to get L_r from the transformer, sectional bobbin is used as shown in Figure 2.17 to put a distance between primary side and secondary side and to increase leakage inductance shown in primary side [34]. Winding construction, number of turns of both sides and length of distance between both windings are key factors once determining L_r value. In addition, air gap between primer and seconder side and turn number of primary winding affects L_m strongly. Various types of cores can be used but PQ and EE types of core are generally used in high power applications.

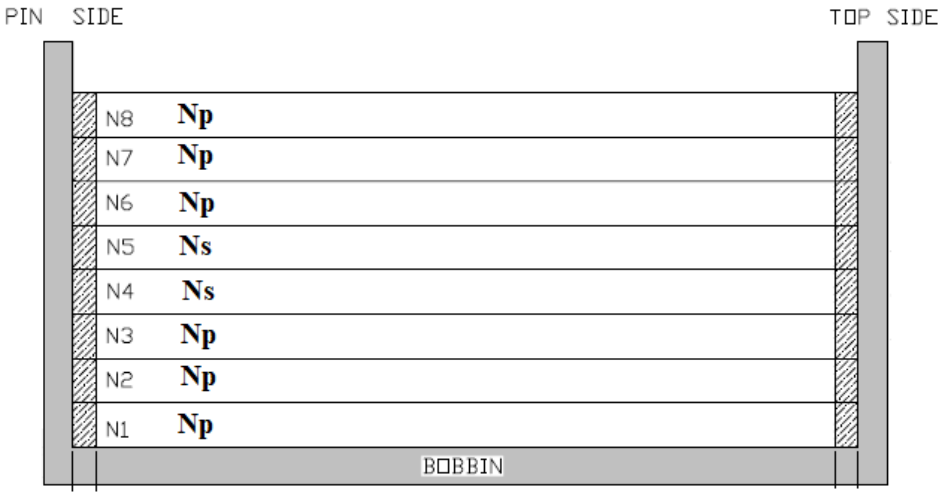

Figure 2.16: Bobbin without primer-seconder section

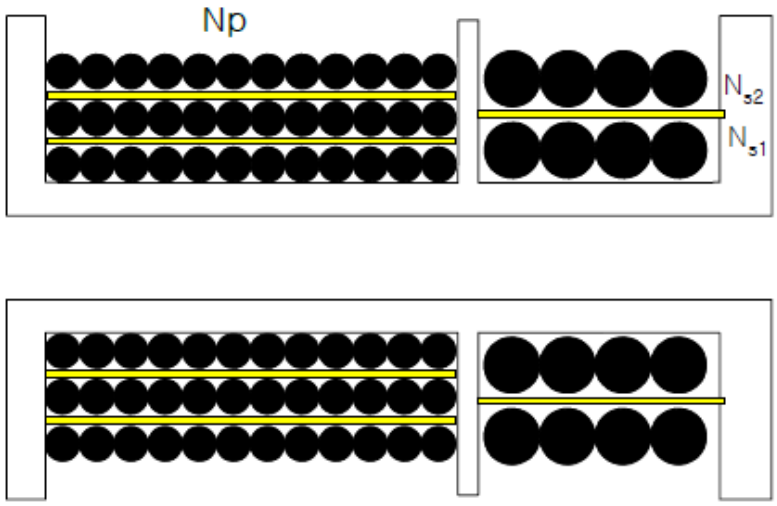

Figure 2.17: Sectional Bobbin

Equation (2.35) shows the minimum turn number for the primary side. Maximum dc gain occurs at minimum switching frequency. Here, in order to obtain minimum operating frequency, equation (2.20) is used after plotting the gain vs frequency curve and getting maximum dc voltage gain.

$$N_p{}^{min} = \frac{n.V_{out}}{2f_s{}^{min}.M_v.\Delta B.A_e} \tag{2.36}$$

Where A_e is cross-sectional area of the transformer core its unity is m^2 and ΔB is peak to peak flux density in *Tesla* as can be observed in Figure 2.18 [34].

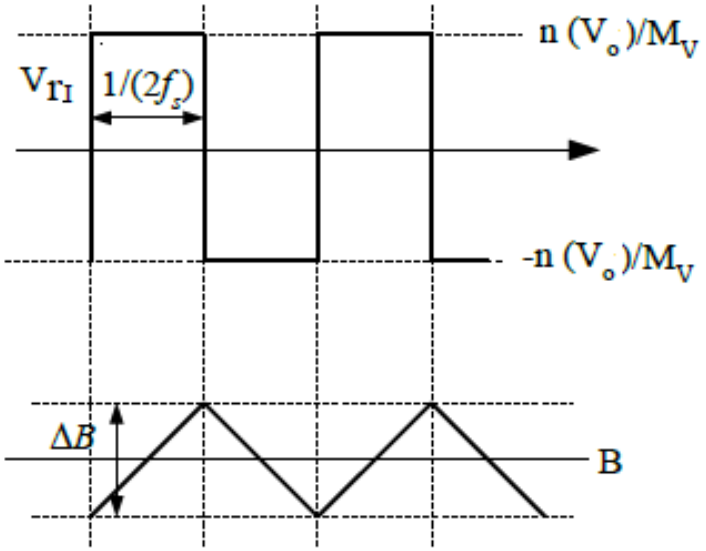

Figure 2.18: Flux density waveform in the transformer

2.2 Conventional Constant On-Time Control Method for LLC Resonant Converter

The filtering behavior of the resonant network circuit implies to apply FHA method to get voltage gain equation of the system where only the fundamental frequency component of input square wave is taken into account.

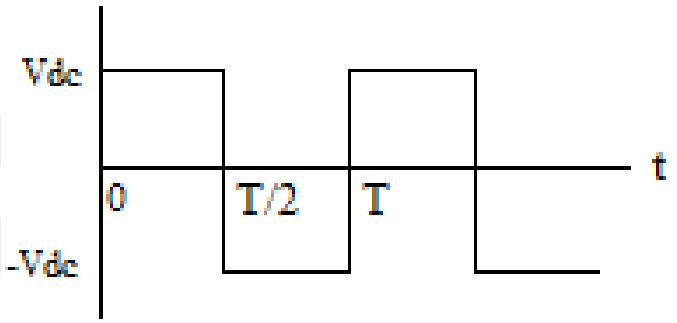

Figure 2.19: A Square wave

Figure 2.19 shows a square wave waveform. Fourier series for the square wave contains odd harmonics and can be described as [39]

$$V(t) = \sum_{n\ odd}\left(\frac{4Vdc}{n\pi}\right)sin(n\omega_0 t) \tag{2.37}$$

Figure 2.20 shows the AC equivalent circuit of the LLC resonant converter shown in Figure 2.1, where $V_{out,F}$ is the fundamental component of the square wave output voltage and $V_{in,F}$ is fundamental component of the square wave input voltage [39]-[41].

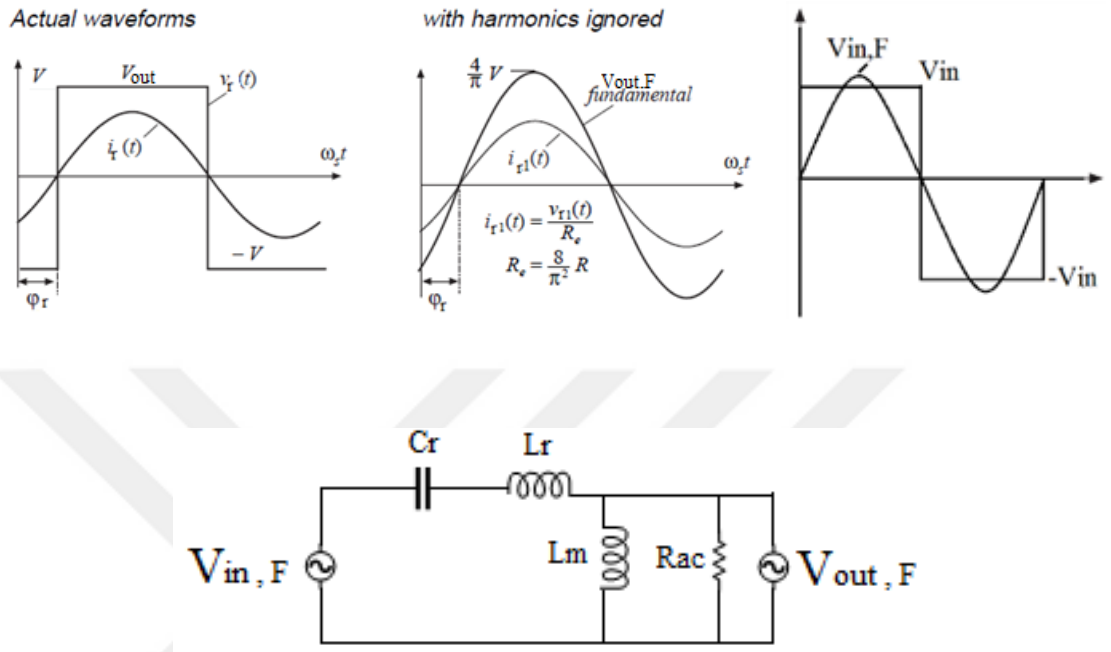

Figure 2.20: AC equivalent circuit of the LLC resonant converter

$$V_{out,F} = \frac{4nV_{out}}{\pi} sin(\omega t) \tag{2.38}$$

$$V_{in,F} = \left(\frac{4V_{in}}{\pi}\right) sin(\omega t) \tag{2.39}$$

Based on the AC equivalent circuit of the LLC converter, the voltage gain ($|M(i\omega)|$) can be derived by circuit analysis [22][39][40][41]. In s domain, the input impedance Z_{in} and output impedance Z_{out} can be found from Figure 2.20 as

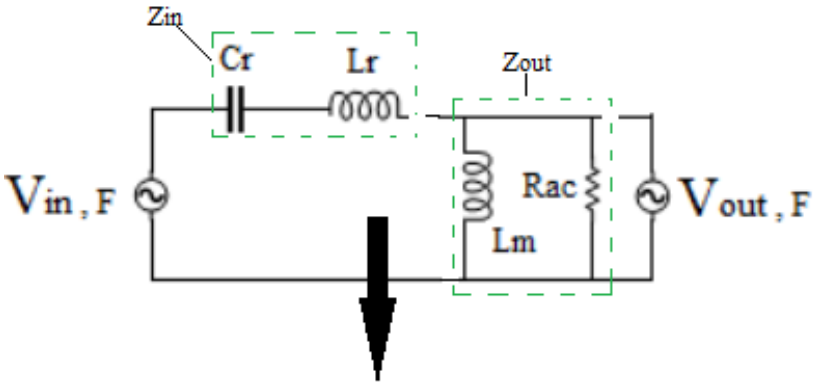

$$Z_{in} = sL_r + \frac{1}{sC_r} \tag{2.40}$$

$$Z_{out} = sL_m // R_{ac} = \frac{sL_m R_{ac}}{sL_m + R_{ac}} \tag{2.41}$$

The voltage gain is defined as

$$M(s) = \frac{V_{out},F(s)}{V_{in},F(s)} = \frac{Z_{out}}{Z_{in}+Z_{out}} \tag{2.42}$$

Therefore, by substituting (2.40) and (2.41) into (2.42), voltage gain in frequency domain can be obtained as

$$|M(i\omega)| = \frac{\left|\left(\frac{\omega}{\omega_0}\right)^2 (m-1)\right|}{\left|\left(\frac{\omega^2}{\omega_p^2}-1\right)+i\left(\frac{\omega}{\omega_0}\right)\left(\frac{\omega^2}{\omega_0^2}-1\right)(m-1)Q\right|} \tag{2.43}$$

where:

$$Q = \sqrt{\frac{L_r}{C_r}}\left(\frac{1}{R_{ac}}\right),\ \omega_0 = \frac{1}{\sqrt{L_r C_r}},\ \ \omega_p = \frac{1}{\sqrt{L_p C_r}},\ \omega = 2\pi f_{sw}.$$

In conventional control method, as observed from (2.43), variable gain is achievable only by changing switching frequency, f_{sw}, since the magnitude of input square wave and resonant network are constant at a specific load condition.

2.3 Proposed Control Method for LLC Resonant Converter

In the proposed method, the converter's switching frequency is constant, and in turn, the voltage gain is also constant. Therefore, in order to adjust the output voltage, the only way is to control the input fundamental voltage magnitude. The simple way to control the fundamental component in an inverter circuit is using modified square wave modulation as shown in Figure 2.21 [39].

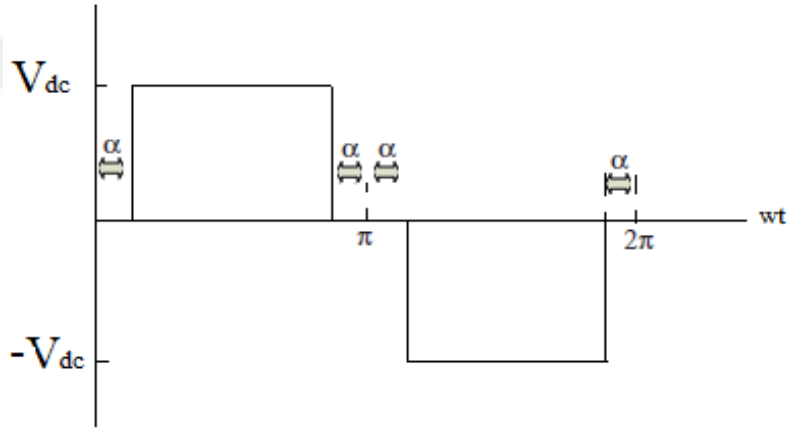

Figure 2.21: A modified square wave

Fourier series of this waveform shown in Figure 2.21 is defined by [39]

$$V(t) = \sum_{n\ odd}\left(\frac{4Vdc}{n\pi}\right)cos(n\alpha)sin(n\omega_0 t) \tag{2.44}$$

where α is the zero (dead) time duration of the voltage at each end of the pulse symmetrically.

As can be seen from (2.44), the fundamental component of the square wave depends on the cosine of α. As a result, even if the voltage gain remains constant at a specific switching frequency, since the amplitude of $V_{in,F}$ shown in Figure 2.20 can be controlled by α, the converter can provide variable output voltage. More specifically, in proposed pulse width control method, the α of the modified square wave signal are controlled precisely until the output voltage reaches the desired level. During this time the switching frequency is kept constant.

2.4 Loss Analysis of Proposed and Control Method for LLC Resonant Converter

In a power circuit, actually switching devices for example diodes and transistors are not ideal even though all assumptions generally are made with ideal switches to simplify calculations and to well define. Voltage drops over MOSFETs, IGBTs and diodes affects significantly thermal performance of a converter. It causes that power losses on the switching devices and reduction of the converter efficiency when current flows through the devices.

In addition to on-state losses due to voltage drops in a switch, switching losses also have to be taken into account when it turns on and turns off. Figure 2.22 shows the two possible scenarios for the switches during switching transition [39].

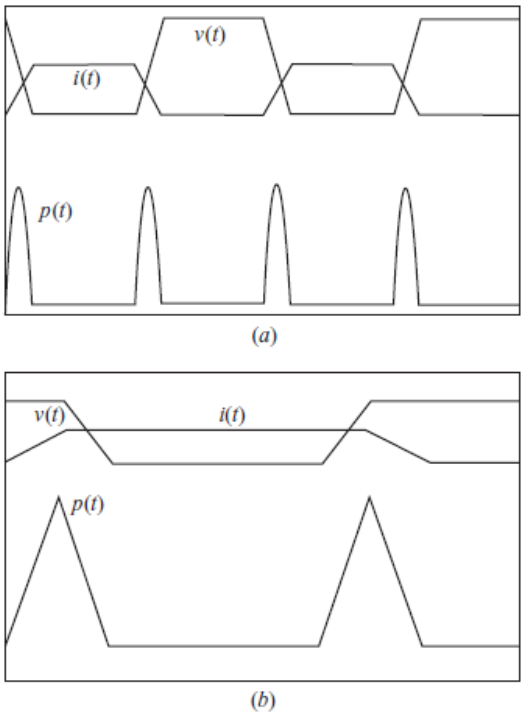

Figure 2.22: Switching transition of a switch and associated power a) Symmetrical transition b) Worst-case condition for on-off transition

Here, Figure 2.22-a illustrates the simultaneous voltage and current waveforms for a switch. It also shows instantaneous power that occurs during transition. Figure 2.22-b shows the waveforms which are not symmetrical. Switching transition illustrated in Figure 2.22-b can generally exist in actual on-off transition. As can be seen in that Figure, switching losses in crossing area is larger than occurs in first condition. Since the average power loss is are under instantaneous power curve divided by the switching period, higher switching frequency means higher switching losses. In order to reduce these losses, one way is that allow converter operate under ZVS or ZCS which is aim of the resonant converters.

2.4.1 Power Losses in Proposed Control Method

Figure 2.23 illustrates typical switching transition for the MOSFETs [44].

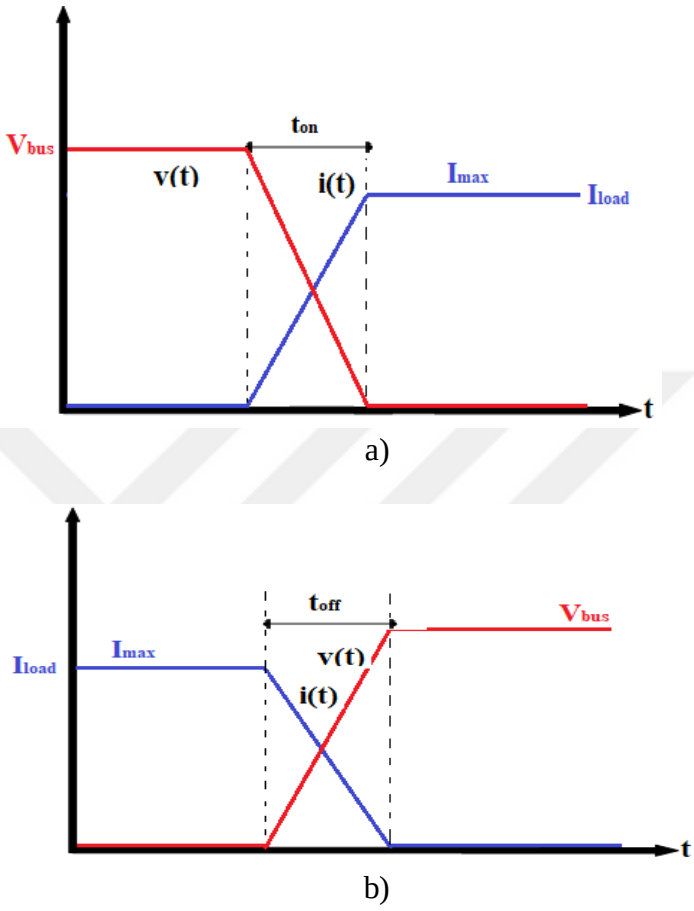

Figure 2.23: Typical switching transition of a MOSFET a) turn-on b) turn-off

MOSFET losses can be divided into switching loss, conduction loss and the MOSFET body diode loss which are denoted by P_{sw}, P_{cond} and P_{diode} respectively. The total loss of a MOSFET can be described as [42]:

$$P_{mosf} = P_{sw} + P_{cond} + P_{diode} \tag{2.45}$$

Switching loss of a MOSFET can be further divided into two section turn on and turn-off loss which is denoted by $P_{sw,on}$ and $P_{sw,off}$ respectively.

For the body diode, there are conduction losses and turn-off losses denoted by $P_{diode,cond}$ and $P_{diode,off}$ respectively. Reverse recovery of the body diode is reason of the turn off loss. But since the voltage across the body diode is nearly zero during reverse recovery, $P_{diode,off}$ is eliminated. Total loss can be extended as [42]:

$$P_{mosf} = P_{sw,on} + P_{sw,off} + P_{cond} + P_{diode,cond} \tag{2.46}$$

The relation between switching losses and energies is defined as [42]

$$P_{sw,on} = E_{sw,on} f_{sw} \tag{2.47}$$

$$P_{sw,off} = E_{sw,off} f_{sw} \tag{2.48}$$

Here, $E_{sw,on}$ is turn on energy and $E_{sw,off}$ is turn off energy of a MOSFET during switching transition.

The rest of the losses are derived as following steps [42]-[44];

$$E_{sw,on} = \int_0^{t_{on}} v(t) i(t) dt$$

where $i(t) = I_{max}\left(\frac{t}{t_{on}}\right)$; $v(t) = V_{bus}\left(1 - \left(\frac{t}{t_{on}}\right)\right)$

$$E_{sw,on} = \frac{V_{bus} I_{max} t_{on}}{6} \tag{2.49}$$

$$E_{sw,off} = \int_0^{t_{off}} v(t)i(t)dt$$

where $v(t) = V_{bus}(\frac{t}{t_{off}})$; $i(t) = I_{max}\left(1 - \left(\frac{t}{t_{off}}\right)\right)$

$$E_{sw,off} = \frac{V_{bus}I_{max}t_{off}}{6} \tag{2.50}$$

$$P_{cond} = I_{mosf,rms}^2 . R_{ds,on} \tag{2.51}$$

where $I_{mosf,rms}$ is the RMS value of the MOSFET drain-source current and $R_{ds,on}$ is drain-source resistance during MOSFET is on.

$$P_{diode,cond} = I_{diode,mean} . V_f \tag{2.52}$$

where $I_{diode,mean}$ is the mean value of the diode current and V_f is forward voltage of the diode.

2.4.2 Power Losses in Conventional Control Method

In conventional method, since the LLC converter allows to operate under ZVS, $E_{sw,on}$ and $P_{diode,off}$ are eliminated. Therefore, total MOSFET loss can be found as

$$P_{mosf} = P_{sw,off} + P_{cond} + P_{diode,cond} \tag{2.53}$$

CHAPTER III

DESIGN AND ANALYSIS OF LLC RESONANT CONVERTER

3.1 Implementation of the Desing Methodology

Figure 3.1 shows the schematic of designed full-bridge LLC resonant converter where L_{m1}, L_{m2}, L_{m3} and L_{m4} are the magnetizing inductances for each transformer. Resonant tank consists of L_{r1},…,L_{r8} and C_r which are the resonant inductances and resonant capacitance respectively.

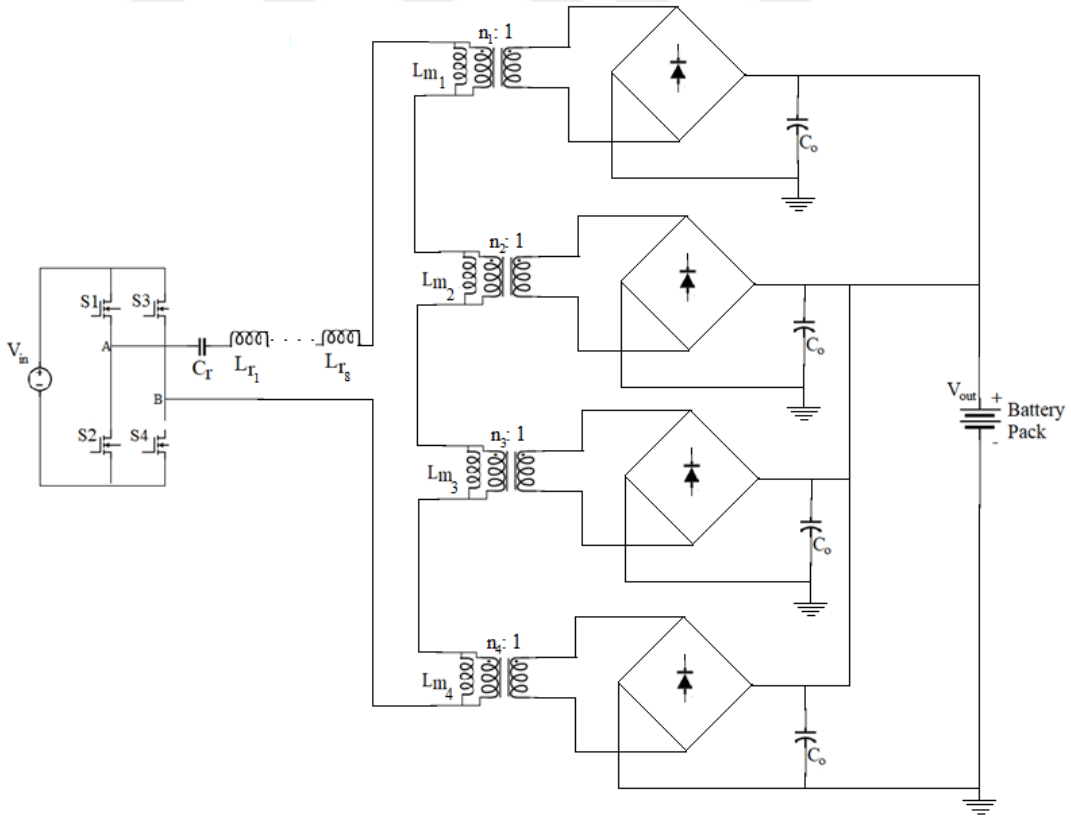

Figure 3.1: Schematic of the proposed system

Transformer and resonant inductor contribute to power transfer in the converter. Since resonant current directly flows through the transformer and resonant inductance in primary side, conduction loss due to impedance of winding components and therefore thermal requirements becomes unavoidable parameters. In order to meet thermal constraints effectively, current can be reduced by paralleling and stored energy in a passive component can be reduced by dividing required value to smaller parts.

In this application, EE55 core was utilized for the resonant transformer. As shown in Figure 3.1, 4 identical transformers are used instead of a transformer to reduce current flowing through a transformer and to reduce conduction loss in a power transfer line. Thus, total output power is shared equally for each transformer and temperature rise in the EE55 core is limited even under worst case.

For the resonant inductor, PQ3812 core is used. The energy stored in the inductance is directly proportional to inductance value and current flowing through itself. Since the temperature rise in the resonant inductor directly depends to the stored energy, total required inductance value is divided to 8 equal parts in order to suppress temperature rise in the core and winding.

System design specifications can be seen from Table 3.1.

Table 3.1: System design specification of the LLC resonant converter

Parameters	Value
Input Voltage Range, $V_{in,min} \sim V_{in,max}$	340~360 V
Nominal Input Voltage, $V_{in,nom}$	350 V
Output Voltage Range, $V_{out,min} \sim V_{out,max}$	200-500 V
Nominal Output Voltage, $V_{out,nom}$	350 V
Maximum Output Power, $P_{out,max}$	7.5 kW
Resonant Frequency, f_{res}	114 kHz

Based on the target system design specifications provided above, full load condition at nominal output voltage is designed to operate at resonant frequency whose voltage gain is close to unity. Design methodology introduced in 2nd section is used in calculations during design stage and following presents these steps respectively.

1) Determine system specifications

$V_{in,min}$, $V_{in,max}$, $V_{out,min}$, $V_{out,max}$, $V_{in,nom}$ and $V_{out,nom}$ have been provided in Table 3.1. System efficiency of 98 % is targeted for this application.

2) **Obtain transformer turns ratio**

$$n = \frac{V_{in,nom}}{V_{out,nom}} = \frac{350}{350} = 1$$

n is valid only when a transformer is used. In this application, as 4 same transformers are used, the turns ratio of each transformer becomes one-fourth of *n*. Turns ratios are provided in Table 3.2.

3) Define the minimum, maximum and nominal dc voltage gain of the resonant converter

$$M_{max} = \left(\frac{V_{out,max}}{V_{in,min}}\right) n = \left(\frac{500}{340}\right) * 1 = 1.47$$

$$M_{min} = \left(\frac{V_{out,min}}{V_{in,max}}\right) n = \left(\frac{200}{360}\right) * 1 = 0.5556$$

$$M_{nom} = \frac{V_{in,nom}}{V_{out,nom}} = \frac{350}{350} = 1$$

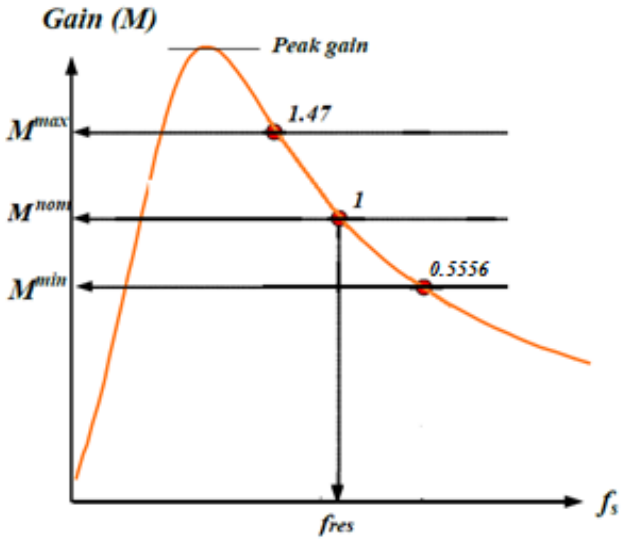

Figure 3.2: Representation of dc gains

4) Calculate the effective load resistance

For the maximum load condition at nominal output voltage, maximum effective load resistance is obtained as:

$$R_e = \left(\frac{8n^2}{\pi^2}\right)\left(\frac{V_{out,nom}^2}{P_o}\right) = \left(\frac{8*1^2}{\pi^2}\right)\left(\frac{350^2}{7500}\right) = 13.25\ \Omega$$

5) Define resonant network component

m defined in 2nd section is ratio of ($L_r + L_m$) to L_r and it is selected as 11. *Q* is quality factor at maximum gain point and it is selected as 0.8. After selecting resonant frequency of 114 kHz defined in Table 3.1, resonant network components are obtained as:

$$C_r = \frac{1}{2\pi Q f_{res} R_e} = \frac{1}{2*3.14*0.8*115000*13.25} \approx 130 \text{ nF}$$

$$L_r = \frac{1}{(2\pi f_{res})^2 C_r} = \frac{1}{(2*3.14*115000)^2 * 130^{-9}} \approx 15 \text{ µH}$$

$$L_p = m * L_r = 11 * 15\ uH = 165 \text{ µH}$$

$$L_m = L_p - L_r = 150 \text{ µH}$$

As seen in Figure 3.1, L_r is divided to 8 equal parts and L_m is divided to 4 equal parts. Table 3.2 shows magnitudes of the components which are used in designed converter.

Table 3.2: Resonant network parameters of the LLC resonant converter

Parameters	Value
Resonant Inductance, $L_{r1} \sim L_{r8}$	1.875 µH
Resonant Capacitance, C_r	128 nF
Magnetizing Inductance of transformer, $L_{m1} \sim L_{m4}$	37.5 µH
Turn ratio, $n_1 \sim n_4$	1/4

Voltage gain curve of the system with respect to switching frequency for various loads can be observed from Figure 3.3.

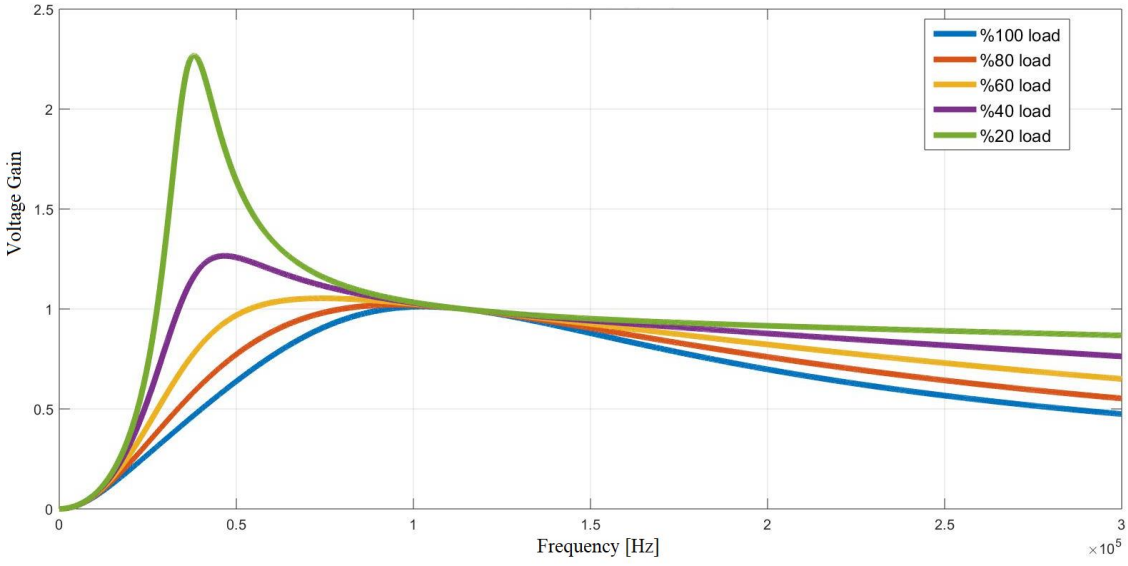

Figure 3.3: Voltage gain curve vs switching frequency

6) Design the transformer of the resonant converter

For the resonant transformer, EE55 core is selected. Winding construction can be seen in Figure 3.4.

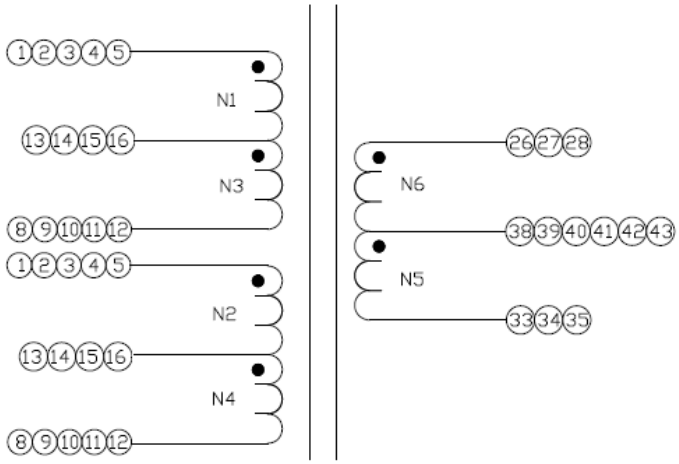

Figure 3.4: Winding construction of the transformer

In addition, LITZ Wire has been chosen to eliminate the skin effect and proximity effect losses in conductors used in the transformer. The winding specification for each layer is given in Figure 3.5.

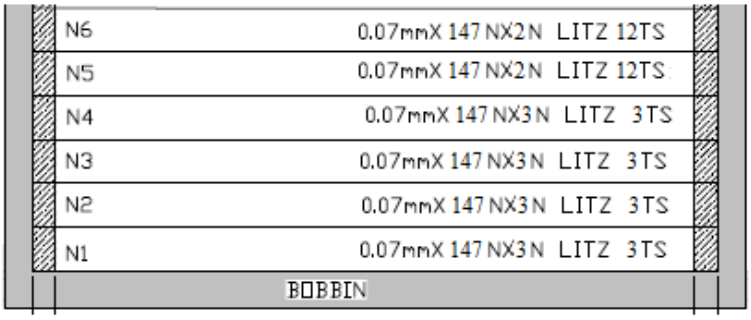

Figure 3.5: Winding specification of the transformer

The layers N1-N2 and N3-N4 are primary windings and are connected in series to achieve 6 turns number on the primary side, but each winding pair is parallel in itself. Similar to primary windings, N5 and N6 layers are secondary windings and they are connected in parallel to obtain 24 turns number for seconder side. Air gap length between main parts of EE55 core that is 0.1 mm is arranged to get primer inductance value of 150 µH. Electrical characteristics of the transformer are depicted in Figure 3.6.

Parameter	Terminals	Criteria
Inductance	L(1,2,3,4,5-8,9,10,11,12)	37.5 uH±10%
Leakage inductance	LK(1,2,3,4,5-8,9,10,11,12) Short Other	0.65uH MAX

Figure 3.6: Electrical characteristics of the transformer

For the resonant inductor, PQ3812 core is selected and winding specification can be seen in Figure 3.7. A total of 8 resonant inductors, each one is 1.8 µH, are used to obtain around 15 µH inductance value in the converter. Magnetic flux flowing in air gap between main parts of the core can cause magnetic interference resulting the EMI and thermal problems upon the cores and the windings especially in high output power operations [45]. In order to reduce magnetic interference, the winding should be placed to be far from the air gap [45]. The magnitude of magnetic interference is reversely proportional to the air gap length [45]. The gap have to be big enough as much as to reduce electromagnetic interference [45].

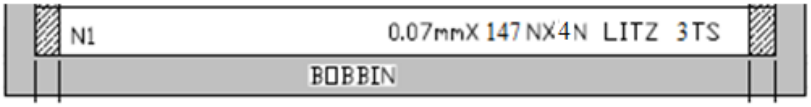

Figure 3.7: Winding specification of the resonant inductor

3.2 Improved Soft Start Characteristics with Proposed Method

In conventional soft starting, since the switching frequency is inversely proportional to the voltage gain of the system, it starts up with high frequency to get low voltage gains and then the switching frequency starts to decrease progressively until output voltage is set. This is very important to prevent the power circuit from inrush current and overshoot of the output voltage. However, high switching frequency operation may not be enough sometimes to suppress inrush current and voltage spikes during start up because of fast transients, stray inductors and parasitic capacitors of layout and devices in the circuit.

Figure 3.8-a shows the output voltage and the resonant tank current with conventional soft start. Here, the initial value of switching frequency is 150 kHz and the final value is 100 kHz with constant dead time of 1us. While Figure 3.8-b and Figure 3.8-c show the waveforms for transient points at switching frequency of 150 kHz and 114 kHz respectively, Figure 3.8-d shows the waveforms for steady state operation its switching frequency of 100 kHz.

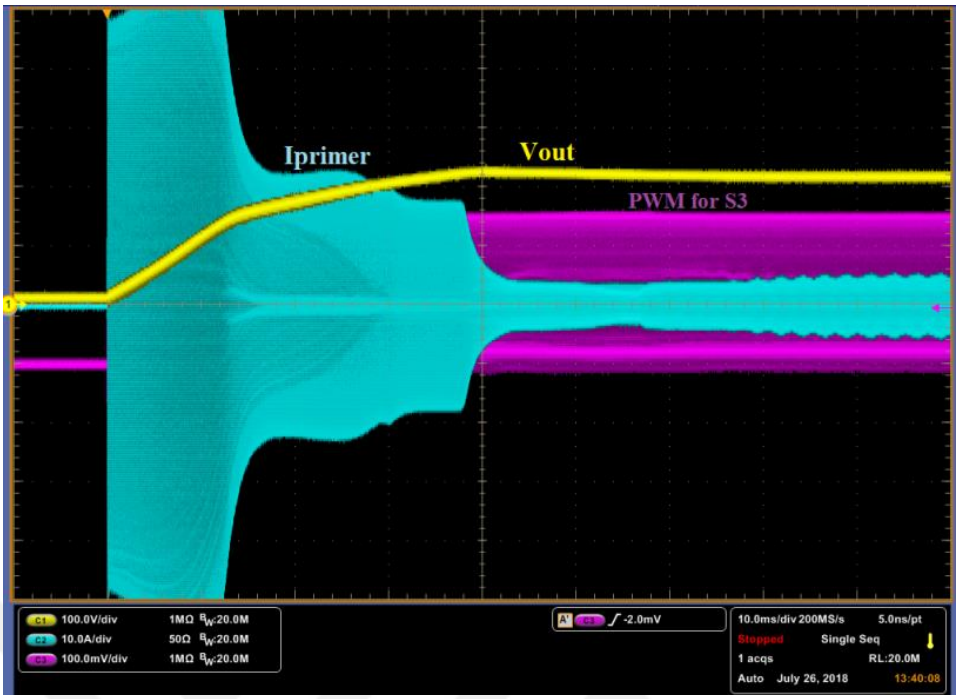
Iprimer
Vout
PWM for S3
C1 100.0V/div 1MΩ BW:20.0M
C2 10.0A/div 50Ω BW:20.0M
C3 100.0mV/div 1MΩ BW:20.0M
-2.0mV
10.0ms/div 200MS/s 5.0ns/pt
Stopped Single Seq
1 acqs RL:20.0M
Auto July 26, 2018 13:40:08

a)

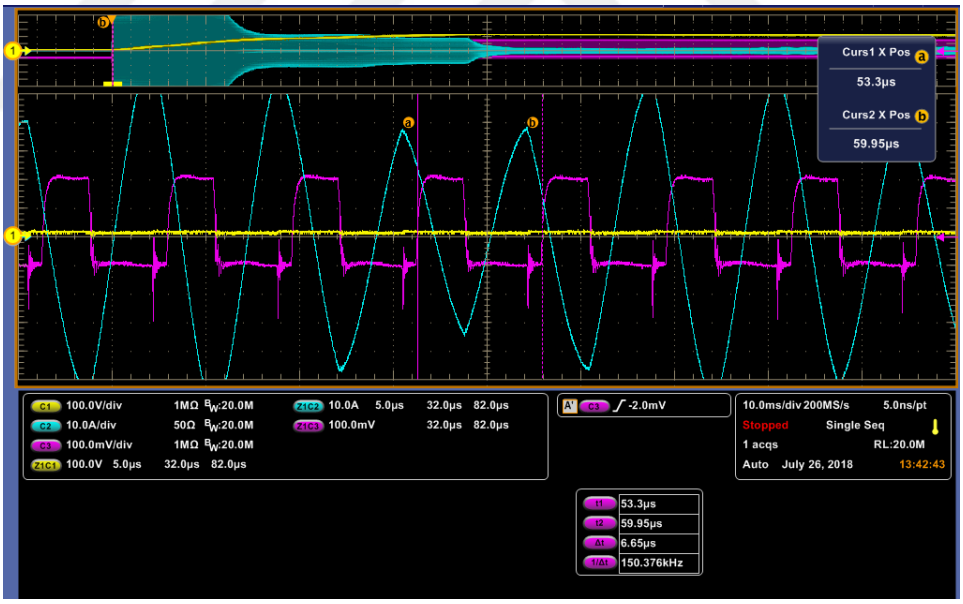
Curs1 X Pos a
53.3µs
Curs2 X Pos b
59.95µs
C1 100.0V/div 1MΩ BW:20.0M
C2 10.0A/div 50Ω BW:20.0M
C3 100.0mV/div 1MΩ BW:20.0M
Z1C1 100.0V 5.0µs 32.0µs 82.0µs
Z1C2 10.0A 5.0µs 32.0µs 82.0µs
Z1C3 100.0mV 32.0µs 82.0µs
-2.0mV
10.0ms/div 200MS/s 5.0ns/pt
Stopped Single Seq
1 acqs RL:20.0M
Auto July 26, 2018 13:42:43
t1 53.3µs
t2 59.95µs
Δt 6.65µs
1/Δt 150.376kHz

b)

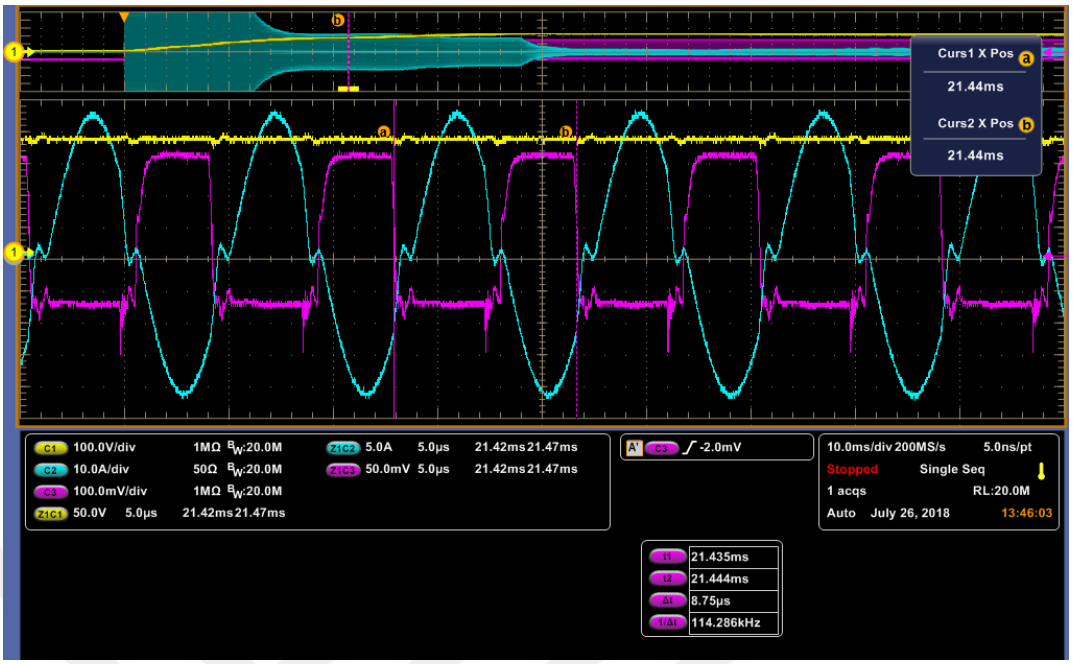

c)

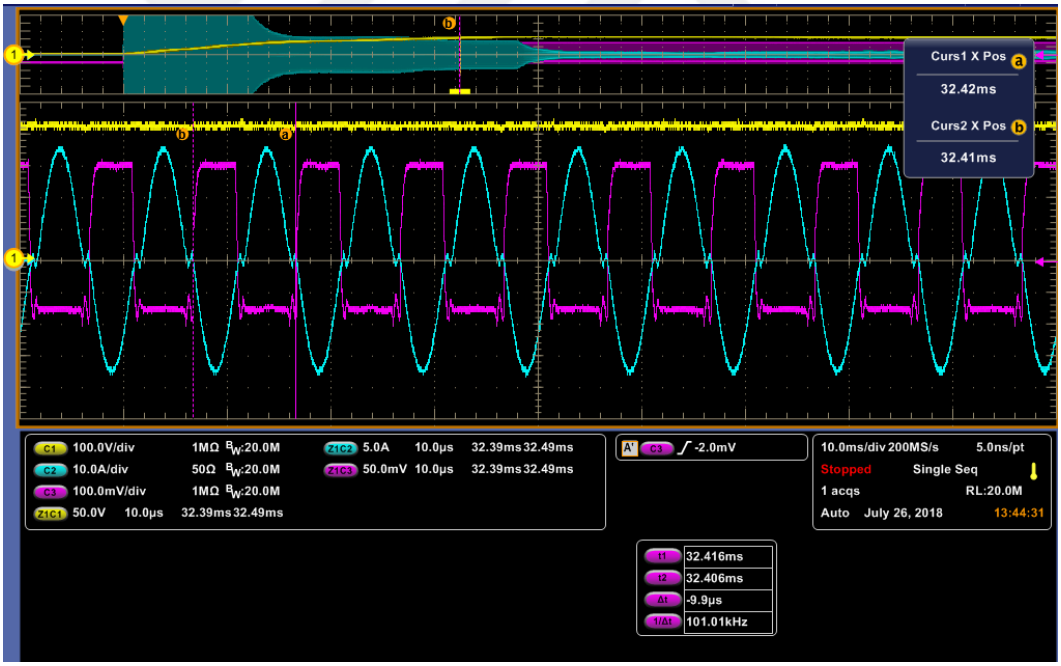

d)

Figure 3.8: Soft start waveforms with conventional method V_{in}= 200 V, V_{out}=200 V, P_{out}=500 W
a) General view b) Waveforms @150 kHz c) Waveforms @114 kHz d) Waveforms @100 kHz

In proposed method, the system starts with minimum duty ratio and it rises progressively by keeping the switching frequency constant until output voltage is established. Since initial on time of switching components are minimum, inrush current are not observed at start up. Soft start for both primer current and output voltage are obtained by increasing on time of pulses progressively.

Figure 3.9-a shows the output voltage and the resonant tank current during start up with proposed method. Here the system has constant switching frequency of 100 kHz. Soft start is implemented by decreasing α from 5 µs to 1 µs gradually. While Figure 3.9-b and Figure 3.9-c show the waveforms at transient points, Figure 3.9-d shows the waveforms at steady state operation.

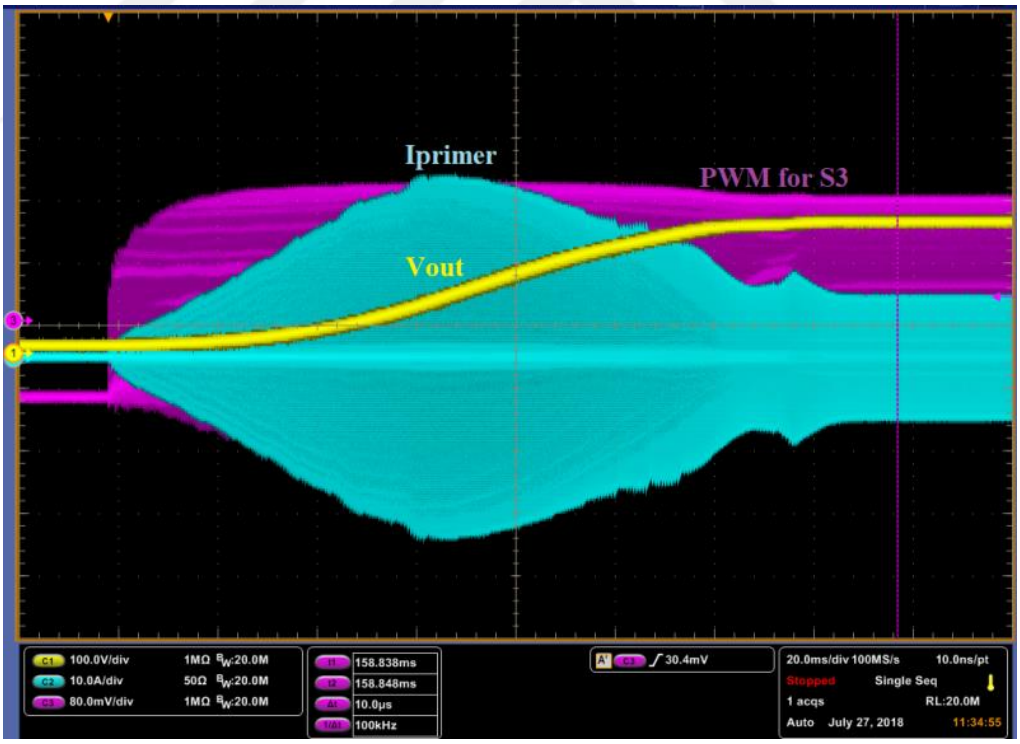

a)

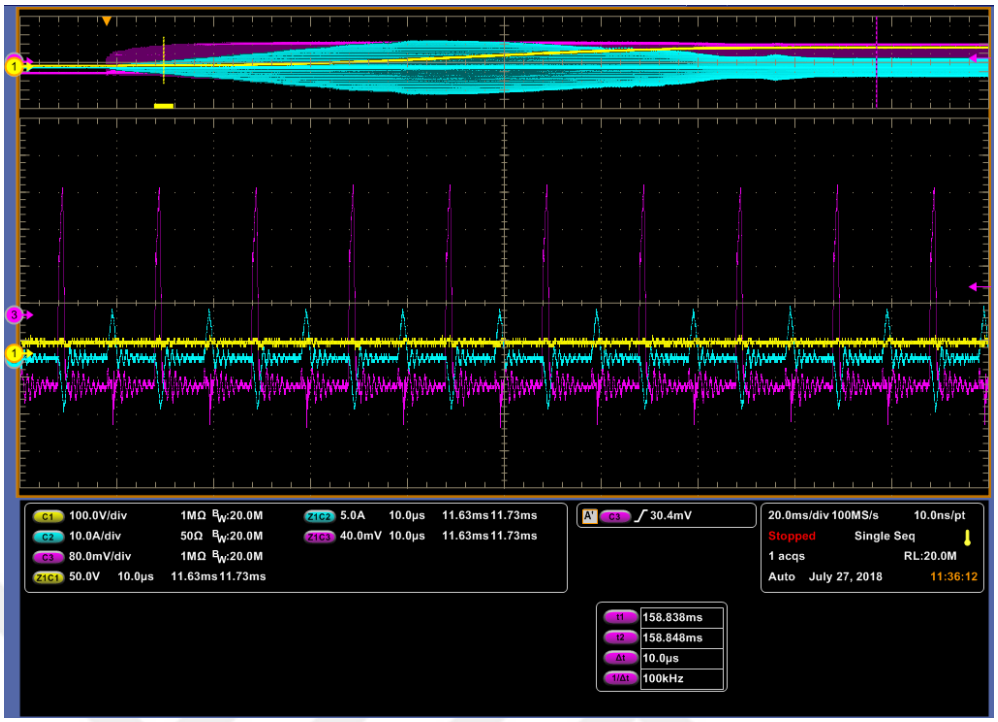
C1 100.0V/div 1MΩ BW:20.0M
C2 10.0A/div 50Ω BW:20.0M
C3 80.0mV/div 1MΩ BW:20.0M
Z1C1 50.0V 10.0µs 11.63ms 11.73ms
Z1C2 5.0A 10.0µs 11.63ms 11.73ms
Z1C3 40.0mV 10.0µs 11.63ms 11.73ms
A' C3 30.4mV
20.0ms/div 100MS/s 10.0ns/pt
Stopped Single Seq
1 acqs RL:20.0M
Auto July 27, 2018 11:36:12
t1 158.838ms
t2 158.848ms
Δt 10.0µs
1/Δt 100kHz

b)

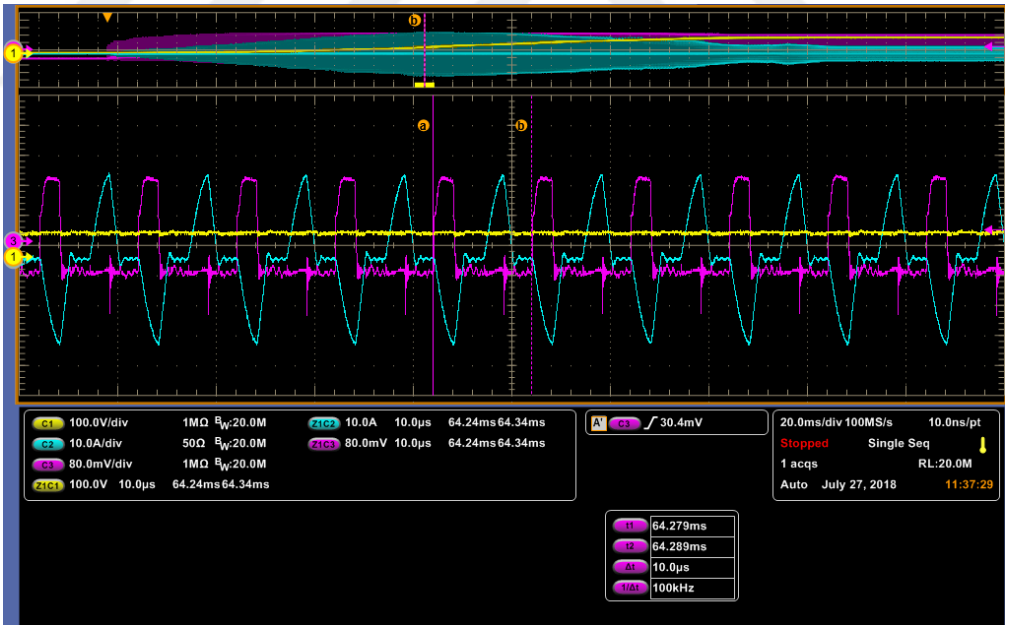
C1 100.0V/div 1MΩ BW:20.0M
C2 10.0A/div 50Ω BW:20.0M
C3 80.0mV/div 1MΩ BW:20.0M
Z1C1 100.0V 10.0µs 64.24ms 64.34ms
Z1C2 10.0A 10.0µs 64.24ms 64.34ms
Z1C3 80.0mV 10.0µs 64.24ms 64.34ms
A' C3 30.4mV
20.0ms/div 100MS/s 10.0ns/pt
Stopped Single Seq
1 acqs RL:20.0M
Auto July 27, 2018 11:37:29
t1 64.279ms
t2 64.289ms
Δt 10.0µs
1/Δt 100kHz

c)

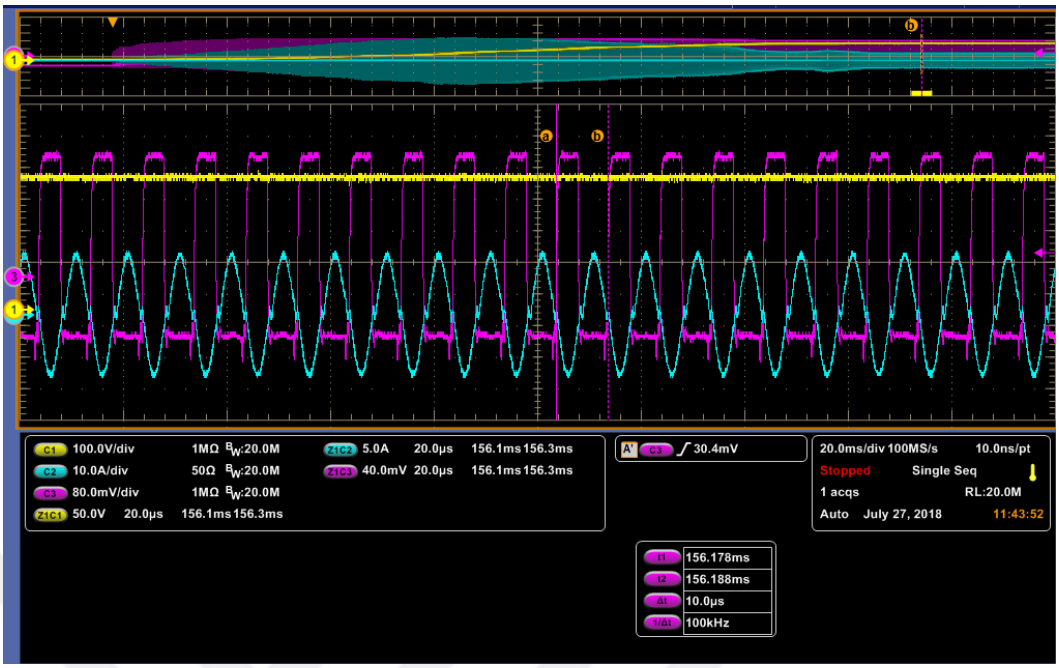

d)

Figure 3.9: Soft start waveforms with proposed method V_{in}= 200 V, V_{out}=200 V, P_{out}=1 kW
a) General view b) Waveforms @10ms 100 kHz c) Waveforms @65ms 100 kHz d) Waveforms @156ms 100 kHz

As a result, the inrush current is not observed during soft start at 1 kW load thanks to proposed method. However excessive inrush current is observed in conventional method even though it is tested with 500W load which is the half of the proposed method load.

3.3 Loss Comparison of a Low Side MOSFET for Both Methods

To verify advantage of the proposed method in terms of the MOSFET losses, the full bridge LLC resonant converter has been built based on the specification in Table 3.1 and Table 3.2. Figure 3.10 shows the experimental prototype of the converter. Teledyne LeCroy MDA810A and Tektronix DPO 7104C oscilloscopes are used for the measurements.

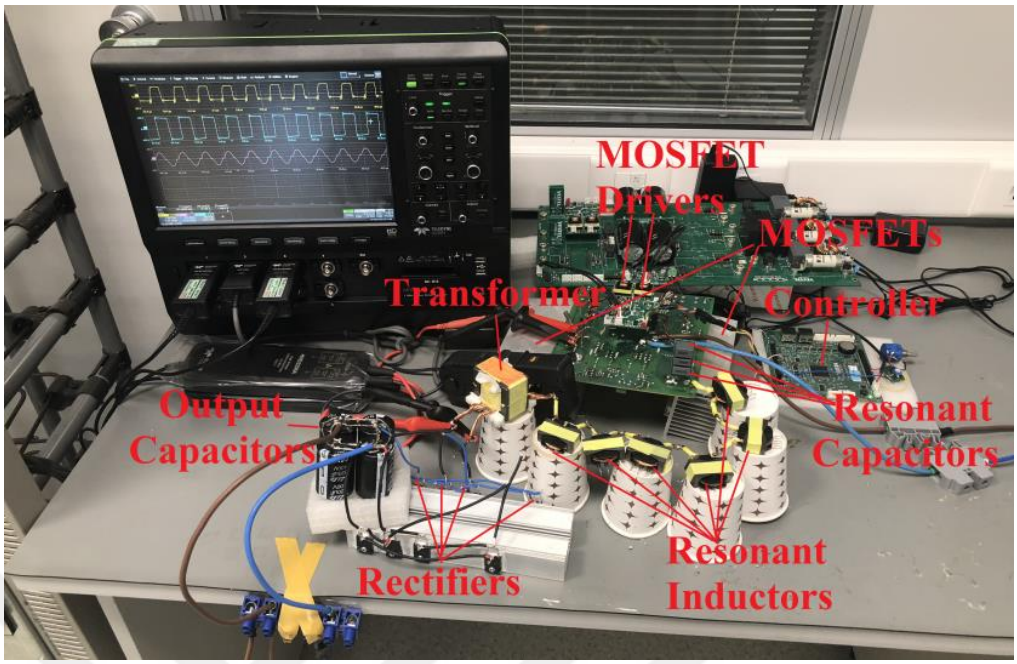

Figure 3.10: Experimental prototype

A commercial MOSFET is selected and its associated parameters are tabulated in Table 3.3 for both methods.

Table 3.3: The Selected Mosfet Parameters for Loss Comparison

FMW60N027S2FDHF	
Parameters	**Value**
Maximum Drain-Source Voltage	600 V
Continuous Drain Current	60 A
Turn-on time	100 ns
Turn-off time	(50-100)ns
Drain-Source On-State Resistance	0.04 Ω
Diode Forward On-Voltage	1.35 V

Figure 3.11 shows the waveforms at output voltage of 160 V and output power of 1600 W using conventional method whose dead time of 1 µs and switching frequency of 130 kHz. Here, the drain-source and gate-source voltages of the S2 MOSFET in Figure 3.1 and resonant tank primer current can be observed. It is denoted by V_{ds}, V_{gs} , and I_{primer} respectively.

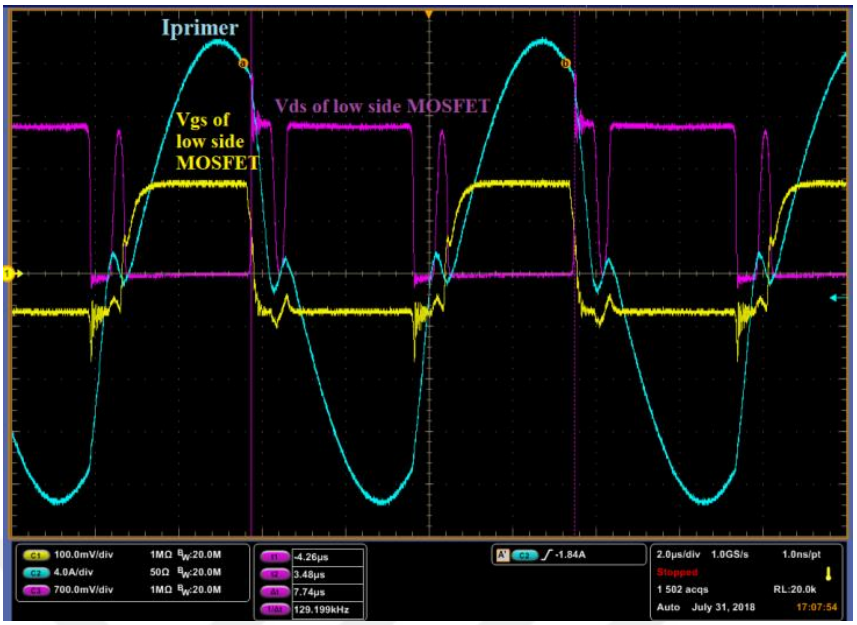

Figure 3.11: S2 drain-source voltage, gate input voltage and primer current with conventional method @ P_{out} =1600 W, V_{out}=160 V, f_{sw}=130 kHz, α=1 µs

The same operating condition mentioned above is obtained thanks to proposed method by implementing 80 kHz switching frequency with α=*3.2 µs*. Figure 3.12 shows the related waveforms.

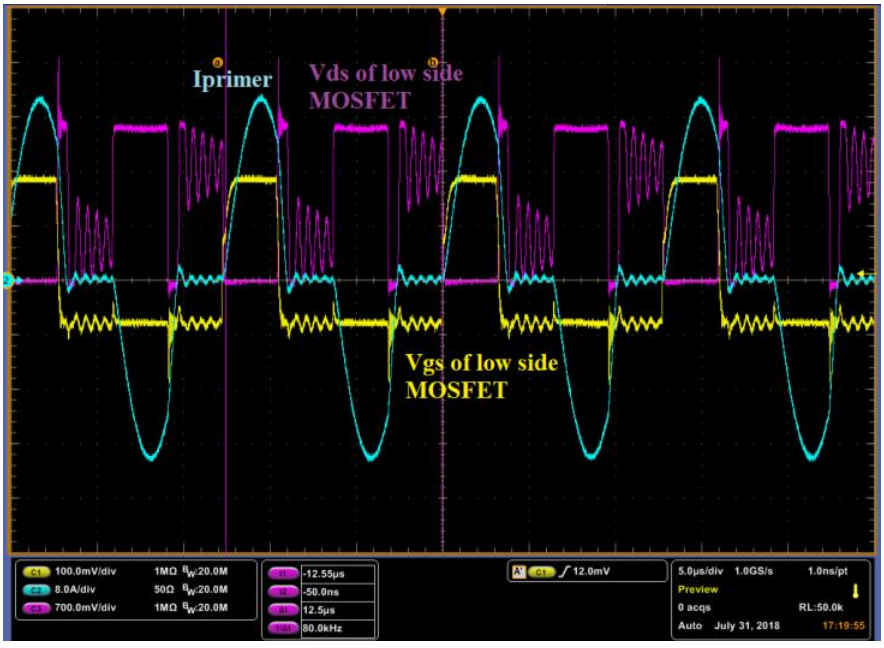

Figure 3.12: S2 drain-source voltage, gate input voltage and primer current with proposed method @ P_{out} =1600 W, V_{out}=160 V, f_{sw}=80 kHz, α=3.2µs

Test steps for both methods are same and provided in Table 3.4. In conventional method, the α time is selected as 1 µs due to dead time requirements against cross-conduction.

Table 3.4: Test Steps for Loss Comparison

	Output Power, $P_{out}[W]$	***Output Voltage,*** $V_{out}[V]$	***Switching frequency,*** $f_{sw}[kHz]$	***Dead time,*** α
Conventional Method	1500	216	195	1µs
	3100	308	130	1µs
	7500	350	100	1µs
	6000	360	90	1µs
	5000	370	85	1µs
	2500	405	75	1µs
Proposed Method	1500	216	80	4.2µs
	3100	308	80	3.2µs
	7500	350	80	2.2µs
	6000	360	80	1.8µs
	5000	370	80	1.5µs
	2500	405	80	900ns

Based on the test conditions given in Table 3.4, Figure 3.13 illustrates the comparison results of the calculated losses of a low side MOSFET in the prototype by using theoretical loss analysis characterized in Section II for both proposed and conventional methods.

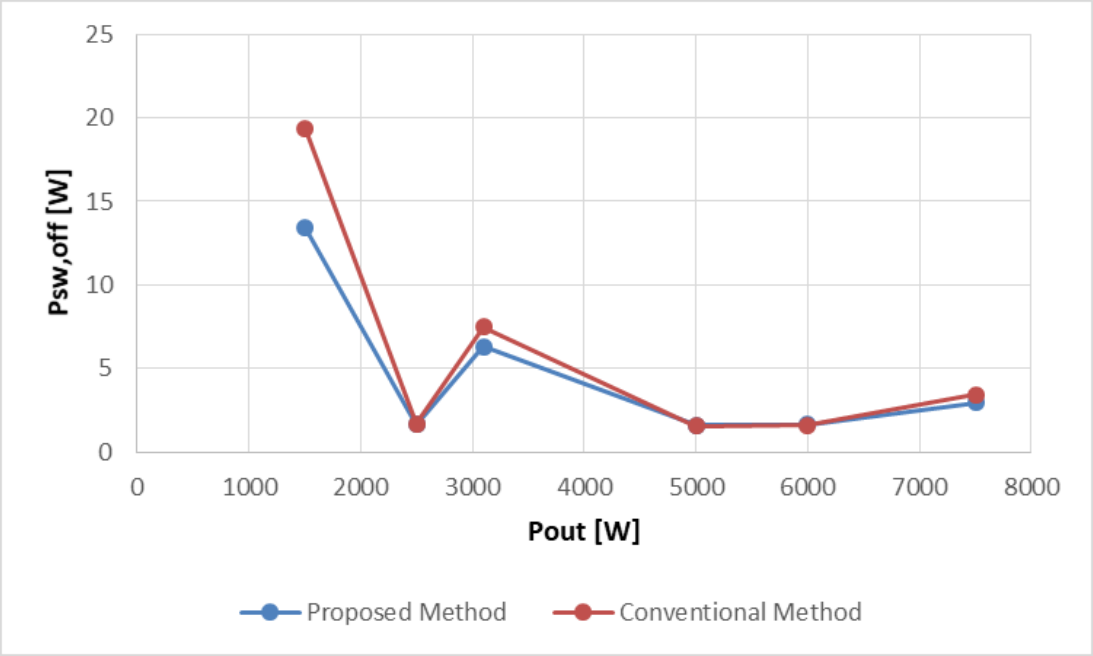
25
20
15
10
5
0
Psw,off [W]
0
1000
2000
3000
4000
5000
6000
7000
8000
Pout [W]
Proposed Method
Conventional Method

a)

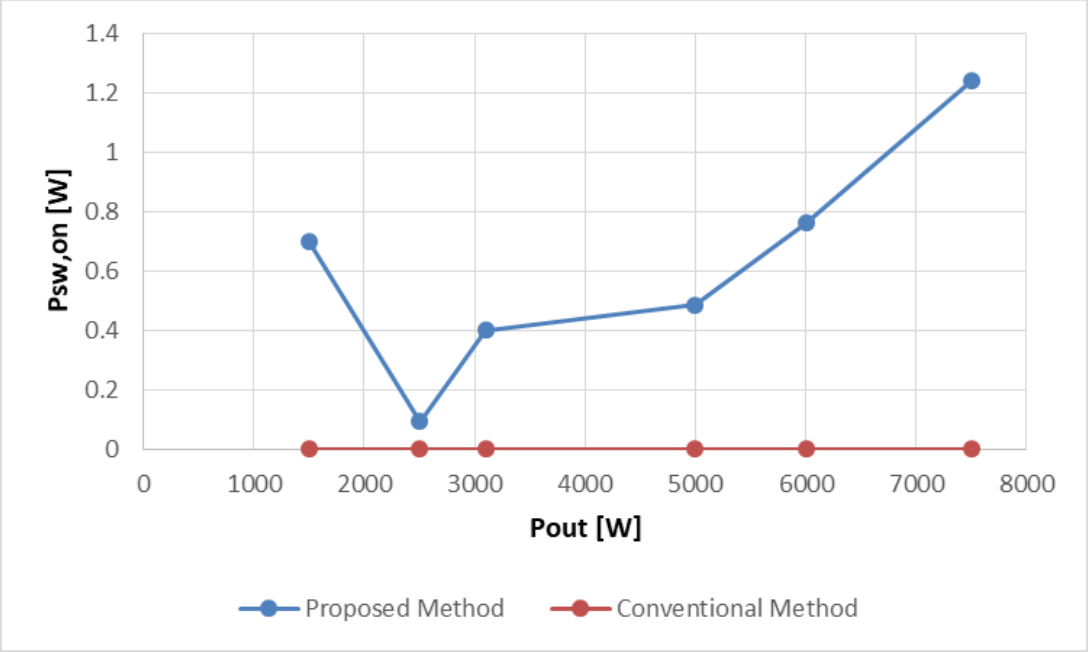
1.4
1.2
1
0.8
0.6
0.4
0.2
0
Psw,on [W]
0
1000
2000
3000
4000
5000
6000
7000
8000
Pout [W]
Proposed Method
Conventional Method

b)

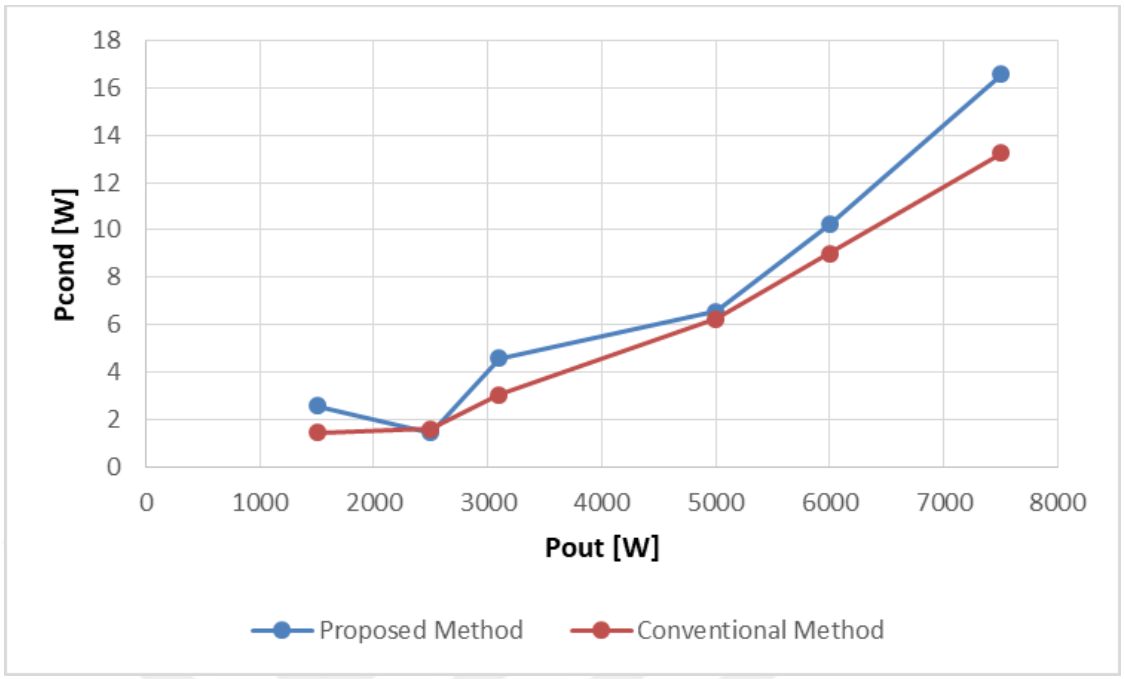
18
16
14
12
10
8
6
4
2
0
Pcond [W]
0
1000
2000
3000
4000
5000
6000
7000
8000
Pout [W]
Proposed Method
Conventional Method

c)

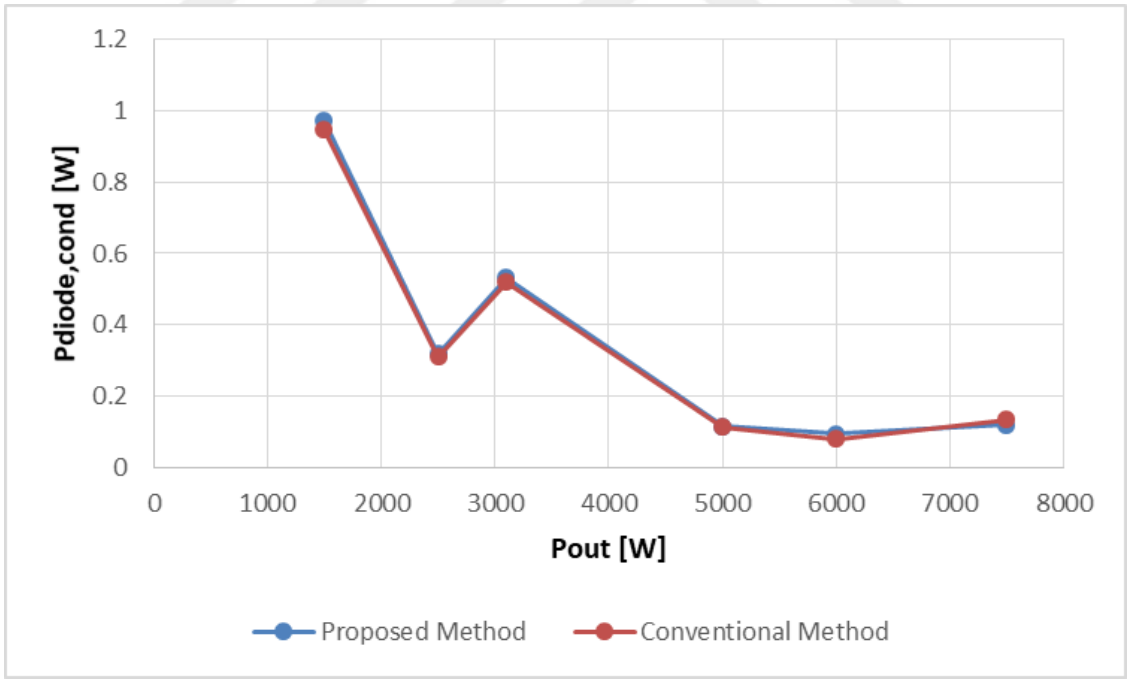
1.2
1
0.8
0.6
0.4
0.2
0
Pdiode,cond [W]
0
1000
2000
3000
4000
5000
6000
7000
8000
Pout [W]
Proposed Method
Conventional Method

d)

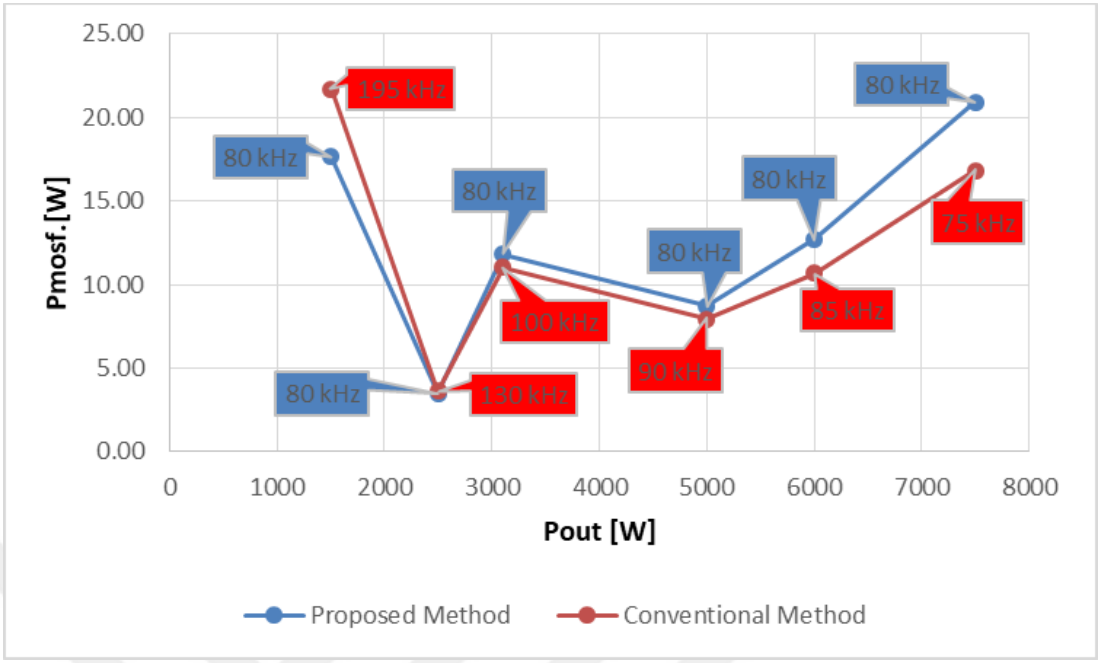

e)

Figure 3.13: Loss comparison of the conventional and proposed method
a) Turn off loss vs output power
b) Turn on loss vs output power
c) Conduction loss vs output power
d-) Conduction loss of the body diode vs output power
e) Total loss of the MOSFET vs output power

Figure 3.13-a shows comparison of the MOSFET turn off losses, $P_{sw,off}$, for two control methods. Turn off loss is directly depend on switching frequency. While the low output voltage levels are achieved at low switching frequency by adjusting α in proposed method, the same voltages are produced at high switching frequencies in conventional method. It can be clearly observed that the proposed method provides significant reduction of switching losses of the MOSFET especially when the system needs low output voltages.

It can be clearly observed from Figure 3.13-b that since the LLC converter allows ZVS operation in conventional control method, $P_{sw,on}$ can be neglected. Even though hard switching can occur with proposed method, $P_{sw,on}$ is negligible due to operation under low switching frequency.

In proposed method, since the converter is operated with maximum dead time values when the low output voltage and low output power levels are required, P_{cond} becomes higher compared to conventional method. Figure 3.13-c shows comparison of it according to two methods.

Since the $I_{diode,mean}$ value in conventional method is same as the values in the proposed method at each step, $P_{diode,cond}$ is almost equal for both methods. It can be clearly seen from Figure 3.13-d

As a result, Figure 3.13-e shows the total losses of the MOSFET at each output power levels for two methods. From this figure, it is clearly seen that proposed method is more efficient especially at light loads requiring low output voltages. For this application resonant converter rated efficiency of 98 % is targeted.

In addition to, the proposed method is investigated in terms of the power factor performance at different loads and a comparison has been made. Consequently thanks to PFC circuit, power factor remains almost equal with both methods at same output power levels (power factor is 0.821 with conventional method and 0.8178 with proposed method). Figure 3.14 shows the grid voltage and current at output voltage of 170 V and output power of 1.8 kW for both methods.

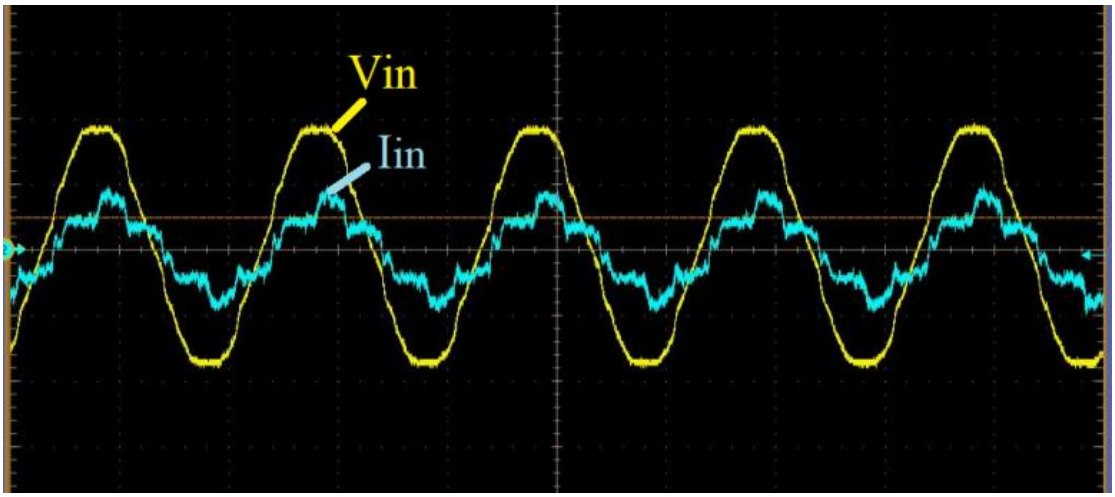

a)

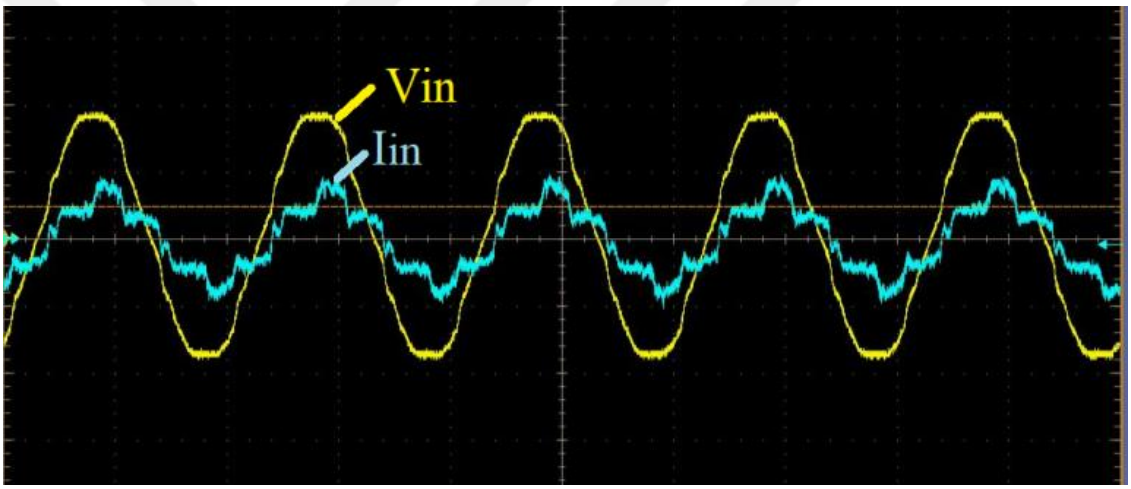

b)

Figure 3.14: Measured AC waveforms
a) Measured Input Voltage and Input Current of classic control
b) Measured Input Voltage and Input Current of proposed control

CHAPTER IV

CONCLUSION

A novel PWM control method for the full bridge LLC resonant converter targeting a wide output voltage source for EV battery chargers has been proposed. Based on the FHA analysis, a design methodology which evaluates the system specifications and provides accurate values of the parameters in the resonant tank is introduced. Characterization of the both proposed and conventional method is presented theoretically in detail. Although the voltage gain is controlled by adjusting the switching frequency in the classical approaches, it is also controllable with pulse width control method in proposed approach. Thanks to this particular method, a variable voltage gain without changing the switching frequency provided significant advantages such as improvement of the soft start characterization and reduction of the switching losses. A design prototype is developed for the demonstration of the idea. It is illustrated that due to minimum on-time of the MOSFET driving signal at the start up, excessive inrush current is suppressed during soft start compared to such adversities in conventional methods. In order to obtain low output voltage levels, unlike the conventional method, the proposed method ensures important loss reduction by implementing low switching frequency via gradually increasing duty ratio for the switch devices. Loss calculations and comparisons show that system efficiency can be better through the targeted approach when the system operates at low output voltage levels. With the help of this study, a more efficient and reliable resonant converter could be designed with the proposed method which may lead the research for future applications.

APPENDIX A

MATLAB CODE FOR PLOTTING DC VOLTAGE GAIN

```
% Matlab code for plotting dc voltage gain versus switching frequency curve

clear all

clc

%system specification

Vin_max=360;

Vin_min=340;

Vin_nom=350;

Vout_min=200;

Vout_max=500;

Vout_nom=350;

Pout_max=7500;

Iout_max=Pout_max/Vout_nom;

Rout=Vout_nom/Iout_max;

m=11;

Q=0.8;

f_res=114000;

%define transformer turns ratio

n=(Vin_nom/Vout_nom);

%minimum and maximum voltage gain of the resonant network

M_nom = 1;

M_max = (Vout_max/Vin_min)*n;
```

```
M_min=(Vout_min/Vin_max)*n;
%equivalent load resistance
Rac_max=((8*n^2)/pi^2)*Rout;
%Resonant Network
Cr=1/(2*pi*Q*f_res*Rac_max);
Lr=1/((2*pi*f_res)*(2*pi*f_res)*Cr);
Lp=m*Lr;
Lm=Lp-Lr;%Lm calculation
wo=1/sqrt(Lr*Cr);
wp=1/sqrt(Lp*Cr);
f=0:50:300e3;
s=1i*2*pi.*f;                    % Complex s variable
Zout=Rac_max.*Lm.*s./(Rac_max+Lm.*s); % Parallel impedance in AC equivalent
circuit
Zin=Lr.*s + 1./(Cr.*s);          % Series impedance in AC equivalent circuit
MM=abs(Zout./(Zin+Zout));     % DC gain
plot(f,MM)                       %100 load
hold on
Ro=(100/80)*Rout;                %80 load
Rac=((8*n^2)/pi^2)*Ro;
Zout=Rac.*Lm.*s./(Rac+Lm.*s);
Zin=Lr.*s + 1./(Cr.*s);
MM=abs(Zout./(Zin+Zout));
plot(f,MM)
hold on
```

```
Ro=(100/60)*Rout;                %60 load
Rac=((8*n^2)/pi^2)*Ro;
Zout=Rac.*Lm.*s./(Rac+Lm.*s);
Zin=Lr.*s + 1./(Cr.*s);
MM=abs(Zout./(Zin+Zout));
plot(f,MM)
hold on
Ro=(100/40)*Rout;                %40 load
Rac=((8*n^2)/pi^2)*Ro;
Zout=Rac.*Lm.*s./(Rac+Lm.*s);
Zin=Lr.*s + 1./(Cr.*s);
MM=abs(Zout./(Zin+Zout));
plot(f,MM)
hold on
Ro=(100/20)*Rout;                %20 load
Rac=((8*n^2)/pi^2)*Ro;
Zout=Rac.*Lm.*s./(Rac+Lm.*s);
Zin=Lr.*s + 1./(Cr.*s);
MM=abs(Zout./(Zin+Zout));
plot(f,MM)
hold on
grid
xlabel('Frequency [Hz]')
ylabel('Voltage Gain')
legend('%100 load','%80 load','%60 load','%40 load','%20 load')
```

BIBLIOGRAPHY

[1] Z. Menyang, Y. Yan, and C. C. Mi, "Analytical approach for the power management of blended-mode plug-in hybrid electric vehicles," IEEE Trans. Veh. Technol., vol. 61, no. 4, pp. 1554–1566, May 2012.

[2] Salman Habib, Muhammad Mansoor Khan, Khurram Hashmi, Muhammad Ali, Houjun Tang, "A Comparative Study of Electric Vehicles concerning Charging Infrastructure and Power Levels'', International Conference on Frontiers of Information Technology, pp.327-332, 2017.

[3] Falvo MC, Sbordone D, Devetsikiotis M., "EV charging stations and modes: international standards,'' In: Power Electronics, Electrical Drives, Automation and Motion (SPEEDAM), International Symposium on. IEEE, pp. 1134–1139,2014.

[4] O. Veneri, L. Ferraro, C. Capasso, D. Iannuzzi, "Charging Infrastructures for EV: Overview of Technologies and Issues, '' 2012 Electrical Systems for Aircraft, Railway and Ship Propulsion, pp.1-6, 2012.

[5] Electric Vehicle Conductive Charging System - Part 1: General Requirements, IEC 61851-1, 2001.

[6] A. Wintrich, U. Nicolai, W. Tursky and T. Reimann, "Application Manual Power Semiconductors," ISLE Verlag, Semikron International, 2011.

[7] M. Claessens, et. al., "Traction Transformation," pp. 11-17, ABB Review, 1/2012.

[8] M. Pavlovsky, "Electronic DC Transformer with High Power Density," PhD Dissertation, Delft University of Technology 2006.

[9] M. Hartmann, "Ultra-Compact and Ultra-Efficient Three-Phase PWM Rectifier Systems for More Electric Aircraft," PhD Dissertation, ETH Zurich, Diss. ETH No. 19755, 2011.

[10] F. Renken and R. Knorr, "High temperature electronic for future hybrid powertrain application," Proceedings of European Conference on Power Electronics and Applications, pp. 1-7, 2005.

[11] F. Krismer, "Modeling and Optimization of Bidirectional Dual Active Bridge DC-DC Converter Topologies, PhD Dissertation, ETH Zurich, Diss. ETH No. 19177, 2010.

[12] M. Yilmaz and P. T. Krein, "Review of Battery Charger Topologies, Charging Power Levels, and Infrastructure for Plug-In Electric and Hybrid Vehicles," IEEE Transactions on Power Electronics, vol. 28, no. 5, pp. 2151-2169, May 2013.

[13] F. C. Schwarz, "A Method of Resonant Current Pulse Modulation for Power Converters," IEEE Transactions on Industrial Electronics and Control Instrumentation, vol. IECI-17, no. 3, pp. 209-221, May 1970.

[14] F. C. Schwarz, "An Improved Method of Resonant Current Pulse Modulation for Power Converters," IEEE Transactions on Industrial Electronics and Control Instrumentation, vol. IECI-23, no. 2, pp. 133-141, May 1976.

[15] R. L. Steigerwald, "High-Frequency Resonant Transistor DC-DC Converters," IEEE Transactions on Industrial Electronics, vol. IE-31, no. 2, pp. 181-191, May 1984.

[16] P. C. Theron and J. A. Ferreira, "The Zero Voltage Switching Partial Series Resonant Converter," IEEE Transactions on Industry Applications, vol. 31, no. 4, pp. 879-886, July/August 1995.

[17] M. Pavlovsky, "Electronic DC Transformer with High Power Density," PhD Dissertation, Delft University of Technology 2006.

[18] R W. De Doncker and J. P. Lyons, "The auxiliary resonant commutated pole converter," Conference Record of the 1990 IEEE Industry Applications Society Annual Meeting,1990, vol. 2, pp. 1228-1235.

[19] F. C. Schwarz, "A Method of Resonant Current Pulse Modulation for Power Converters," IEEE Transactions on Industrial Electronics and Control Instrumentation, vol. IECI-17, no. 3, pp. 209-221, May 1970.

[20] F. C. Schwarz, "An Improved Method of Resonant Current Pulse Modulation for Power Converters," IEEE Transactions on Industrial Electronics and Control Instrumentation,vol. IECI-23, no. 2, pp. 133-141, May 1976.

[21] R. L. Steigerwald, "High-Frequency Resonant Transistor DC-DC Converters," IEEE Transactions on Industrial Electronics, vol. IE-31, no. 2, pp. 181-191, May 1984.

[22] R. W. Erickson and D. Maksimovic, "Fundamentals of Power Electronics," 2nd edition, Kluwer Academic Publishers, 2001.

[23] N. Mohan, T. M. Undeland and W. P. Robbins, "Power Electronics," 2nd edition, John Wiley and Sons, 1995.

[24] B. Yang, "Topology Investigation for Front End DC/DC Power Conversion for Distributed Power System," PhD Dissertation, Virginia Polytechnic Institute and State University, 2003.

[25] R. P. Severns, "Topologies for Three-Element Resonant Converters," IEEE Transactions on Power Electronics, vol. 7, no. 1, pp. 89-98, January 1992.

[26] A. K. S. Bhat and S. B. Dewan, "Analysis and Design of a High-Frequency Resonant Converter Using LCC-Type Commutation," IEEE Transactions on Power Electronics, vol. PE-2, no. 4, pp. 291-300, October 1987.

[27] K.-H. Liu, R. Oruganti and F. C. Y. Lee, "Quasi-Resonant Converters-Topologies and Characteristics," IEEE Transactions on Power Electronics, vol. PE-2, no. 1, pp. 62-71, January 1987.

[28] K.-H. Liu and F. C. Lee, "Zero-voltage switching technique in DC/DC converters," IEEE Transactions on Power Electronics, vol. 5, no. 5, pp. 293-304, July 1990.

[29] B. Yang, "Topology Investigation for Front End DC/DC Power Conversion for Distributed Power System," PhD Dissertation, Virginia Polytechnic Institute and State University, 2003.

[30] M.-C. Tsai, "Analysis and implementation of a full-bridge constant-frequency LCC-type parallel resonant converter," IEE Proceedings-Electric Power Applications, vol. 141, no.3, pp. 121-128, May 1994.

[31] Y. Qiu et. al., "A high-frequency high-efficiency three-level LCC converter for highvoltage charging applications," 2004 IEEE 35th Annual Power Electronics Specialists Conference, 2004, PESC 04, vol. 6, pp. 4100-4106.

[32] L. Bing, L. Wenduo, L. Yan, F. C. Lee, and J. D. van Wyk, "Optimal design methodology for LLC resonant converter," in Proc. 21st Annu. IEEE APEC Expo., 2006, pp. 533–538.

[33] Canales, F., Barbosa, P., Lee, F.C., "A wide input voltage and load output variations fixed-frequency ZVS DC/DC LLC resonant converter for high-power applications,"Proc.IEEE IAS, 2002,vol.4, pp.2306–2313.

[34] H. Choi, “Half-Bridge LLC Resonant Converter Design Using FSFR-Series Fairchild Power Switch (FPS™),” On Semi. Application Note (AN4151), October 2014.

[35] Q. Chen, J. Wang, Y. Ji, S. Liang, “Soft starting strategy of bidirectional LLC resonant DC-DC transformer based on phase-shift control,” IEEE Conference on Industrial Electronics and Applications, 2014, pp. 318-322.

[36] Toshiba, “MOSFET Avalanche Ruggedness,” Application Note, November 2017.

[37] D.Schleisser, D.Ahlers, M.Eicher, M. Pürschel, “Repetitive avalanche of automotive MOSFETs,” European Conference on Power Electronics and Applications (EPE), 2013, pp. 1-7.

[38] Yeh Ting, “DC-DC Converters with a Wide Load Range and a Wide Input-Voltage Range,” Doctoral Dissertation, Delft University of Technology, 2015.

[39] Daniel W.Hart, “Power Electronics,” Valparaiso University 2011.

[40] J.Deng, S.Li, S.Hu, C.C.Mi, R.M, “Design Methodology of LLC Resonant Converters for Electric Vehicle Battery Chargers,” IEEE Transactions on Vehicular Technology, vol. 63, no. 4, pp. 1581-1592, may 2014.

[41] X.Yan, L. Li, Y. Gao, Z. Tao, “Design methodology of LLC converters based on mode analysis for battery charging applications,’’ Annual Conference of the IEEE Industrial Electronics Society, 2017, pp. 1053-1058.

[42] Dr. Dušan Graovac, Marco Pürschel, Andreas Kiep,” MOSFET Power Losses Calculation Using the DataSheet Parameters,” Infineon Application Note, V 1.1, July 2006.

[43] Texas Instruments,” MOSFET power losses and how they affect power-supply efficiency,” Analog Applications Journal, 2016.

[44] Tutorial presentation, “EE368 Power Electronics,” Switching Dissipation and Power Losses.

[45] Prof. Charles R. Sullivan, “High Frequency Magnetics Design: Overview and Winding Loss,” Presentation, Thayer School of Engineering at Dartmouth.

VITA

Yılmaz Daş was born in Izmir/Turkey on 6th May 1991. He received B.Sc. degree of Electrical and Electronics Engineering with the top honor from EGE University in 2014. From 2012 to 2014, he worked as a part-time EMC Engineer at VESTEL Electronics R&D EMC (Electromagnetic Compatibility) Test Laboratory. In July of 2014, he joined the Power Electronics Design team in VESTEL R&D and he is currently working as a hardware design engineer. He has experience to design AC/DC and DC/DC converters for consumer electronics and EV (Electric Vehicle) battery chargers.